JAEA-Research
2024-010
DOI:10.11484/jaea-research-2024-010

JAEA-Research

Multi-Phase Flow Topology and Interfacial Area Model for SIMMER-III and SIMMER-IV

Yoshiharu TOBITA, Satoru KONDO and Koji MORITA

Fast Reactor Cycle System Research and Development Center
Oarai Research and Development Institute

October 2024

Japan Atomic Energy Agency

日本原子力研究開発機構

国立研究開発法人日本原子力研究開発機構　研究開発推進部　科学技術情報課
〒 319-1112　茨城県那珂郡東海村大字村松 4 番地 49
E-mail: ird-support@jaea.go.jp

Multi-Phase Flow Topology and Interfacial Area Model for SIMMER-III and SIMMER-IV

Yoshiharu TOBITA[*1], Satoru KONDO[*2] and Koji MORITA[*3]

Fast Reactor Cycle System Research and Development Center
Oarai Research and Development Institute
Japan Atomic Energy Agency
Oarai-machi, Higashiibaraki-gun, Ibaraki-ken

(Received June 6, 2024)

The multi-component, multi-phase flow topology and interfacial area model has been developed for the SIMMER-III and SIMMER-IV computer codes, which have been extensively used in liquid-metal fast reactor core-disruptive accident analyses. To systematically simulate complex flow topology, flow regime maps are modeled, for both the pool flow and channel flow regimes, with smooth transition between flow regimes. The interfacial area convection model was formulated to enhance the applicability and flexibility of the codes, by tracing the transport and history of interfaces, and thereby better representing transient physical phenomena. The changes of interfacial areas resulting from such as breakup, coalescence, and production of droplets or bubbles were treated as source terms in the interfacial area convection equation.

In a multi-component system of SIMMER-III and SIMMER-IV, all the possible contacts between components are taken into account, and the fluid-to-fluid and fluid-to-structure binary contact areas are prepared for the calculations of heat and mass transfer processes and momentum-exchange functions.

The multi-phase flow topology and interfacial area model developed in this study was the first of a kind as a fast reactor safety analysis code. The model has been extensively tested through the code assessment (verification and validation) program, which has demonstrated that many of the problems associated with simplistic modeling in the previous codes were resolved.

Keywords: Multi-component Flow, Multi-phase Flow, Flow Regimes, Interfacial Area Convection, SIMMER-III, SIMMER-IV, V&V, Severe Accidents, CDA, LMFR Safety

*1 Karlsruhe Institute of Technology

*2 Fast Reactor Cycle System Research and Development Center until March 31, 2023

*3 Kyushu University

SIMMER-III及びSIMMER-IVコードの多相流動・境界面積モデル

日本原子力研究開発機構　大洗研究所
高速炉サイクル研究開発センター

飛田　吉春[*1]、近藤　悟[*2]、守田　幸路[*3]

（2024年6月6日受理）

高速炉の炉心崩壊事故解析コードSIMMER-III及びSIMMER-IVの多相流動・境界面積モデルを開発した。複雑な多成分・多相流のトポロジーを体系的に模擬するため、プール流及びチャンネル流に対する流動様式をモデル化するとともに、流動様式の間の円滑な遷移を可能とした。コードの適用性と柔軟性を拡大するために境界面積対流モデルを導入することにより、各流体の境界面積の輸送と履歴を追跡し、それにより過渡現象をより適切に記述できるようになった。流体粒子の分裂・合体、液滴・気泡の生成等の結果生じる境界面積の時間変化は、境界面積対流方程式のソース項としてモデル化した。

SIMMER-III及びSIMMER-IVの多成分系においては成分間の全ての可能な接触モードを考慮し、成分間の熱及び質量移行、運動量交換関数の計算に必要な流体－流体間、流体－構造材間の2成分間接触面積を計算する。

本研究で開発した境界面積モデルは高速炉安全解析コードとしては世界初のものであり、コード検証（V&V）プログラムを通じて幅広くテストを行った結果、従来のコードにおける簡易モデルに伴う問題点の多くを解決できることが示された。

大洗研究所：〒311-1393　茨城県東茨城郡大洗町成田町 4002

*1 カールスルーエ工科大学

*2 高速炉サイクル研究開発センター (2023 年 3 月 31 日迄)

*3 九州大学

Contents

目　次

Nomenclature

Symbols

A	Convectible interfacial area per unit volume
a	Binary-contact area per unit volume, heat transfer area
Bo	Bond number
C	Constant, coefficient
C_{ANG}	Contact angle
D_h	Hydraulic diameter
E_r	Entrainment fraction
E_u	Equilibrium entrainment fraction
e	Specific internal energy
f_B	Volume fraction of liquid-continuous region
f_D	Volume fraction of vapor-continuous region
g	Heat transfer coefficient
g	Gravity acceleration
Ja	Jacob number
$K_{qq'}$	Momentum exchange function between velocity fields q and q'
K_{qS}	Momentum exchange function between velocity field q and structure
k	Thermal conductivity
M_b	Nucleation site density
n	Number density of bubbles
P	Pressure
Q	Specific internal energy generation rate
Re	Reynolds number
r	Radius
S	Source term of convectible interfacial area
u	Radial velocity
v	Axial velocity
v'	Turbulent velocity
$\vec{v}_q$	Velocity (vector) of velocity field q
VM	Virtual mass
We	Weber number
X_B	Fraction of liquid components in liquid-continuous region

X_D	Fraction of liquid components in vapor-continuous region

Greek symbols

α	Volume fraction
$\alpha_{G,eff}$	Effective void fraction
$\alpha_{G,EOS}$	Real void fraction
Γ	Mass transfer rate
μ	Viscosity
τ	Time constant
ϑ_{sup}	Dimensionless superheat
ρ	Microscopic density
$\bar{\rho}$	Macroscopic density
σ	Surface tension
$\chi(s)$	Operator to represent convection of *s*
ω	Coalescence probability

Subscripts and superscripts

B	Bubbly flow region
CL	Coalescence of bubbles
CL	Continuous liquid
CP	Continuous phase
CV	Volume change due to convection
crt	Critical point
D	Dispersed flow region
e	Equilibrium
en	Entrainment
F	Flow
FS	Structure surface to which the liquid film contacts
G	Vapor
L	Liquid
LC	Left can wall
Li	Liquid energy component *i*
li	Liquid density component *i*
MB	Mass transfer to bubbles
N	Nucleation
P	Particle
PIN	Fuel pin

RC	Right can wall
S	Structure
sat	Saturation line
Si	Structure energy component *i*
si	Structure density component *i*
TB	Turbulence breakup
VS	Structure surface to which the liquid film does not contact
WB	Weber breakup

This is a blank page.

1. Introduction

The SIMMER-III and SIMMER-IV computer codes couple a two-/three-dimensional, multi-velocity field, multi-phase, multi-component, Eulerian fluid dynamics module with a space- and time-dependent neutronics model and a structure model[1) - 7)]. In order to model complex multi-phase flow physical processes, mass and energy conservation equations are solved for the density components and energy components, respectively. Here SIMMER-IV is the three-dimensional code, which retains essentially the same modeling as two-dimensional SIMMER-III, except for fluid convection algorithm and additional structure wall treatment in SIMMER-IV. In the rest of this report, only the code name SIMMER-III is referred to, unless noted differently.

The codes have been used for simulating complex physical processes of dynamic multi-phase flows during liquid-metal fast reactor (LMFR) core disruptive accidents (CDAs), such as boiling pool dynamics, molten fuel relocation and freezing, and fuel-coolant interactions. These are the phenomena occurring through local heat and mass transfer processes at the interfaces between different materials (or components). The momentum exchange processes occur also at fluid-to-fluid and fluid-to-structure interfaces. These interfacial phenomena are dominated by interfacial areas, which are primarily determined from geometrical configurations (topology) and volume fractions of the fluid and structure components.

In the former SIMMER-II code developed at the Los Alamos National Laboratory[8)], a two-velocity code, a very simple flow regime is modeled, i.e. a dispersed droplet flow is assumed regardless of void fraction, except for a low void fraction range in which a bubbly flow is simulated. Interfacial areas are calculated based on instantaneous local flow conditions alone. In the next step, a significant improvement was made in the Advanced Fluid-Dynamics Model (AFDM) code [9)], a three-velocity-field prototype code, in which the convection of interfacial areas was modeled to better represent transient interfacial phenomena, and multi-phase flow configurations are simulated by 12 flow topologies[10)]. This pioneering effort with AFDM has been successful, even though the code is more or less a research tool and cannot be applied to reactor cases.

The SIMMER-III interfacial area (IFA) model is based on the AFDM approach. As a reactor safety analysis code, full reactor materials are treated with the structure modeling that has been much improved from SIMMER-II. The rather complex multi-phase flow topology treatment in AFDM is simplified to be practicable; however, the treatment of flow regimes affected by structure (called “channel flow”) is modeled in addition to “pool flow”. The IFA convection with source terms is modeled similarly to AFDM and is extended to be consistent with the increased number of fluid components and comprehensive flow regimes. Thus, the SIMMER-III IFA model has the following salient and advanced features:

(1) Multi-phase flow topology treatment: Both the pool flow and channel flow regimes are modeled as flow-regime maps covering an entire vapor volume (void) fraction range from 0 to 1. In those flow regimes for which it is difficult to draw the flow topology, a suitable interpolation procedure is introduced to avoid any abrupt changes in flow properties upon flow regime transition.

(2) Convection of IFA: When a fluid component flows from one cell to a neighboring cell, the surface of the fluid flows as well. This is described by an IFA convection equation and thereby the history of the IFA can be traced. A total of 11 convectible interfacial areas are treated.

(3) IFA source terms: The surface areas of fluids change with time due to dynamic processes such as bubble coalescence and hydrodynamic droplet breakup. The source terms of IFA are defined by an equilibrium value and time constant, and are included in the IFA convection equation.

(4) Binary contact areas: With 8 fluid energy components (7 liquids and 1 vapor mixture) and 3 structure surface components (5 for SIMMER-IV), there are possible 28 fluid-to-fluid binary contacts (28 for SIMMER-IV) and 24 fluid-to-structure contacts (40 for SIMMER-IV). Thus, the total of 52 binary contact areas are calculated in SIMMER-III (68 for SIMMER-IV).

The IFA modeling concept and an early version of the model for SIMMER-III was first documented in the 1990s as an informal technical memorandum and a conference paper.[11] The present report is intended to be a full documentation of the IFA model including the latest improvements and the provisions for SIMMER-IV. In the rest of this report, the fluid-dynamics model of SIMMER-III is briefly presented in Chapter 2 to understand the purpose and importance of the IFA model. The multi-phase flow topology and flow regimes are described in Chapter 3. The IFA convection and source terms are formulated in Chapters 4 and 5, respectively. The binary contact areas for fluid-fluid contacts and fluid-structure contacts are defined in Chapter 6. Although the details of the verification and validation (V&V) of the model is beyond the scope of this report, the achievements of SIMMER-III assessment program with respect to IFA modeling are summarized in Chapter 7. Additional detailed information with respect to the IFA modeling is available in Appendices.

2. Overview of SIMMER-III and Purpose of Interfacial Areas

2.1. Overview of Fluid Dynamics Algorithm

The fundamental mass, momentum and energy equations are written in a differential form as follows. For mass conservation,

$$\frac{\partial \bar{\rho}_m}{\partial t} + \nabla \cdot \left(\bar{\rho}_m \vec{v}_q\right) = -\Gamma_m \,, \tag{2-1}$$

where the mass is represented by the macroscopic density (mass per unit volume) $\bar{\rho}_m$ and Γ_m is the total mass-transfer rate per unit volume from component m. The momentum equation is written as:

$$\begin{aligned}\frac{\partial \bar{\rho}_q \vec{v}_q}{\partial t} + \sum_{m\in q} \nabla \cdot \left(\bar{\rho}_m \vec{v}_q \vec{v}_q\right) + \alpha_q \nabla p - \bar{\rho}_q \vec{g} + K_{qS}\vec{v}_q - \sum_{q'} K_{qq'}\left(-\vec{v}_q\right) - \overrightarrow{\boldsymbol{VM}}_q \\ = -\sum_{q'} \Gamma_{qq'}\left[\mathrm{H}\left(\Gamma_{qq'}\right)\vec{v}_q + \mathrm{H}\left(\Gamma_{q'q}\right)\vec{v}_{q'}\right],\end{aligned} \tag{2-2}$$

where the K_{qS} and $K_{qq'}$ terms on the left side$\vec{v}_{q'}$ are the momentum exchange functions that couple the velocity field q to a different field or structure, and $\overrightarrow{\boldsymbol{VM}}_q$ is the virtual mass term. The energy equation is written below with the energy represented by the specific internal energy of component M.

$$\begin{aligned}\frac{\partial \bar{\rho}_M e_M}{\partial t} + \sum_{m\in M} \nabla \cdot \left(\bar{\rho}_m e_m \vec{v}_q\right) + p\left[\frac{\partial \alpha_M}{\partial t} + \nabla \cdot \left(\alpha_M \vec{v}_q\right)\right] \\ - \frac{\bar{\rho}_M}{\bar{\rho}_m}\left[\sum_q K_{q'q}\left(\vec{v}_q - \vec{v}_{q'}\right)\cdot\left(\vec{v}_q - \vec{v}_{q'}\right) + K_{qS}\vec{v}_q \cdot \left(\vec{v}_q - \vec{v}_{qS}\right) + \overrightarrow{\boldsymbol{VM}}_q \right. \\ \left. \cdot \left(\vec{v}_q - \vec{v}_{GL}\right)\right] = Q_N + Q_M(\Gamma_M) + Q_H(h, a, \Delta T)\,,\end{aligned} \tag{2-3}$$

where the terms on the right-hand side of the equation denote the specific energy sources due to nuclear heating, mass transfer, and heat transfer to energy component M. The detailed explanation of these equations is described in the SIMMER-III/SIMMER-IV report[1)].

The most complex portion of the fluid dynamics is the model for intra-cell heat and mass transfers, which describe the physical phenomena associated with multi-component, multiphase flows. Interactions between different components having different energies take place locally at places where two components come into contact. In the former SIMMER-II, heat and mass exchange rates were determined at the beginning of time step, and the end-of-time-step updates due to convection were calculated assuming these exchange rates stay constant during the time step. The approach taken by SIMMER-II is merited when relatively large time step sizes can be used for quasi-steady-state problems. However, for highly transient cases with rapid phase transition, non-linear phenomena such as vaporization and condensation cannot be accurately and consistently treated. In the past, this limitation of the code produced serious stability and accuracy problems.

The fundamental fluid-dynamics solution algorithm employed in SIMMER-III is time-factorization, four-step method, first developed for AFDM code,[12] in which intra-cell transfer is decoupled from fluid convection. The complexity associated with modeling the various inter-related phenomena of heat and mass transfer is the main reason of selecting this approach. Based on the successful implementation of the algorithm in AFDM, the same solution procedure is adopted in SIMMER-III/SIMMER-IV with extension to multi-component system with full reactor materials and structure configuration. In the four-step algorithm, local phenomena or interactions are treated as intra-cell transfer processes in Step 1, which is decoupled from the fluid inter-cell convection treated in Steps 2-4. Step 1 solves the mass and energy equations without convection terms, and updates the end-of-time-step mesh cell variables resulted from intra-cell heat and mass transfer. Also evaluated in Step 1 are momentum exchange functions to be used in fluid-convection calculations. The individual models of Step 1 are programmed in a modular way such that future improvement or replacement with new models can be implemented easily.

2.2. SIMMER-III/SIMMER-IV Components

All materials are represented by components: density components are used to calculate the mass conservation equations; and energy components the energy conservation equations. The complete lists of the structure-, liquid- and vapor-field components are shown in Tables 1 through 3. In these tables, the lower-case subscripts denote density components while the upper-case subscripts denote energy components. The fuel components are divided into fertile and fissile in their mass (density components) to represent different enrichment zones in the core. However, the two materials are assumed to be intimately mixed, and hence the single temperature is assigned (energy components).

It is noted the only difference between SIMMER-III and SIMMER-IV is the number of can walls; i.e. the front and back can walls are modeled in a three-dimensional code in addition to left and right can walls.

2.3. Purposes of Interfacial Area Model

In the solution algorithm, the intra-cell heat and mass transfer terms are solved in Step 1. For determination of the mass-transfer rates and energy-transfer rates appearing in Eqs. (2-1) and (2-3), the interface condition of the two components exchanging mass and energy is required. For example, the energy-transfer rate due to heat transfer is determined from the binary contact area and the heat-transfer coefficient between the two energy components, which are calculated in the IFA and heat-transfer coefficient (HTC) models, respectively. The momentum exchange functions (MXFs) are also calculated based on the interfacial area between two velocity fields or a velocity field and structure.

A simplified computational flow of Step 1 is depicted in Fig. 1. The IFA model has several purposes. Based on the structure configuration and component volume fractions, a flow regime in each mesh cell is determined. The convectible IFA resulted from fluid convection are updated for source terms. Then the binary contact areas are calculated for all the fluid-to-fluid and fluid-to-structure interfaces.

Heat and mass transfer calculations are performed at each interface based on the calculated binary contact area and the heat-transfer coefficient determined by other modules. The binary contact areas are also used to calculate momentum exchange functions (fluid-to-fluid drag and fluid-to-structure friction), which

are used in solving the momentum equation Steps 2 to 4. Thus, the IFA model is one of the most essential models in simulating multi-phase flows.

3. Multi-Phase Flow Topology and Flow Regimes

Before presenting the individual multi-phase flow regimes, a basic concept is described as to how geometrical configuration (topology) of complex multi-flow flows is represented. Then the convectible interfacial areas are defined, followed by the model description of flow regimes in pool and channel flow topologies.

3.1. Basic Concept of Multi-Phase Flow Representation

In modeling a geometrical configuration of multi-phase flows in SIMMER-III, there are several challenges to confront with. First, the geometrical configurations (topology) of multi-phase, multi-component flows are complex and difficult to describe, and hence bold simplifications are necessary. Second, the model should cover an entire void fraction range from a vapor flow to a single-phase liquid flow. Third, in SIMMER-III, flow regimes are modeled for both a pool flow, in which the effect of the structure is negligible, and a channel flow, which is confined by the structure. Smooth transitions between flow regimes are always desired for avoiding any discontinuity or abrupt changes caused by inadequate modeling.

We will start with a pool flow topology, which is much simpler with no effect of structure. A basic concept of representing the pool flow is a combination of the two flow regimes: a liquid-continuous bubbly flow regime and a vapor-continuous dispersed (droplet) flow regime, as shown in Fig. 2. Between the bubbly and dispersed flow regimes, the transition flow regime is defined to represent the conventional churn-turbulent flow. The transition flow regime is assumed to consist of a bubbly flow region with its local void fraction α_B and a dispersed region with its local void fraction α_D. The volume ratio of these two regions is defined such that an averaged void fraction over the flow area equals the given flow void fraction. The liquid component with the largest volume fraction is assumed to form a continuous phase in the bubbly flow region.

In Fig. 2, the effective void fraction is defined, in the SIMMER-III equation-of-state (EOS) model, by

$$\alpha_{eff} = \max\left[\alpha_0(1-\alpha_S),\ \alpha_{G,EOS} + \alpha_0(\alpha_L + \alpha_P)\right], \tag{3-1}$$

in calculating two-phase pressure. With this definition, smooth transition from a single-phase to two-phase cell is ensured. Since α_{eff} is used in the heat and mass transfer model and hence it should be also used consistently as the vapor volume fraction in the IFA calculation.

Equation (3-1) can be replaced, by a user input option, with the real gas volume fraction with a limiter:

$$\alpha_G = \max\left[\alpha_{G,EOS}, \alpha_{G,Min}\right], \tag{3-2}$$

where $\boldsymbol{\alpha_{G,Min}}$ are input limiters (10^{-3} ~ 10^{-2} may be appropriate as the default values). It is noted that, if we use $\boldsymbol{\alpha_G}$, problems may develop due to inconsistency between the interfacial areas and the volume fraction $\boldsymbol{\alpha_{eff}}$ used in the calculation of heat and mass transfer. Therefore, after the calculation of momentum-exchange functions, the binary contact areas between vapor and the other components are modified based on $\boldsymbol{\alpha_{eff}}$ to keep consistency with the heat and mass transfer calculation. The modification procedure is

$$a_{G,Lm,B}^{eff} = a_{G,Lm,B} + \frac{\alpha_{Lm}}{\alpha_L}\left(A_{G,B,eff} - A_{G,B}\right), \text{ for } m=1, 2, 3, \tag{3-3}$$

where

$a_{G,Lm,B}^{eff}$ is a contact area between vapor and the other component *M* in the bubbly region based on α_{eff}

$a_{G,Lm,B}$ is a contact area between vapor and the other component *M* in the bubbly region based on α_G

$A_{G,B,eff}$ is the convectible area of bubbles based on α_{eff}, and is given by

$$A_{G,B,eff} = A_{G,B}\frac{\alpha_{G,eff}}{\alpha_G}.$$

This procedure violates the "summation rule" that the sum of contact areas over a component should be equal to the convectible interfacial (surface) area of the component,

$$A_M = \sum_{K \neq M} a_{M,K} \tag{3-4}$$

where A_M is a convectible IFA area of the component *M*, and $a_{M,K}$ is a binary contact area of the component *M* with the other component *K*. The inconsistency problem can be resolved by re-calculating binary contact areas based on α_{eff} after the momentum-exchange functions calculation. However, it is decided not to implement this re-calculation in SIMMER-III, unless the above violation is likely to affect the calculated behavior significantly.

3.2. Definition of Convectible Interfacial Areas

A concept of the convection of interfacial area concentration (interfacial area per unit volume) was first proposed by Ishii in the mid-1970s.[13] To implement this concept in a multi-component system, three convectible IFA were modeled in AFDM.[10] In SIMMER-III, with the increased number of fluid energy components, more convectible IFAs must be modeled in a physically consistent way. Before introducing the IFA convection model in Chapter 4, the convectible IFAs of SIMMER-III are defined in this section. The structure surface areas are also described.

3.2.1. Convectible interfacial areas

A basic concept is the convection of the surface areas of associating fluid components. Out of 11 convectible IFAs per unit volume modeled in SIMMER-III, 10 IFAs associating respectively to the energy components are convected. As depicted in Fig. 3, these are:

$A_{Lm,B}$, m=1, 2, 3 : the IFAs of real liquids (fuel, steel, and sodium) in the bubbly region,

$A_{Lm,D}$, m=1, 2, 3 : the IFAs of real liquids in the dispersed region,

A_{Lp}, p=4, 5, 7 : the IFAs of fuel particles, steel particles and fuel chunks, and

$A_{G,B}$, : the IFA of the bubble in the bubbly flow region.

It is noted that the real liquids in the bubbly and dispersed flow regions are distinguished, but the solid components (still in the liquid field) are not distinguished between the two regions. The IFA area for the vapor mixture is treated only as bubble surface area in the bubbly flow region.

In addition, the interface area between the bubbly and dispersed regions, $A_{B,D}$, is defined as an additional convectible IFA. Because of the difficulty in defining a velocity and source terms for $A_{B,D}$, it is not convected actually and is to be defined based on the instantaneous local condition of the flow. A simple approach for pool flow is to use an AFDM approach that $A_{B,D}$ should increase if the bubbles increase in the bubbly region and the liquids increase in the dispersed region. The formula is

$$A_{B,D} = \min(f_B,\ f_D) C_{B,D} \left(A_{G,D} + \sum_{m=1}^{6} A_{Lm,D} \right), \tag{3-5}$$

where f_B and f_D respectively denote the volume fractions of the bubbly (liquid-continuous) and dispersed (vapor-continuous) regions, and $C_{B,D}$ is input multiplier (default value is one).

The IFA of the control particles is not convectible and is obtained instantaneously from the input radius r_{L6}.

$$A_{L6} = \frac{3\alpha_{L6}}{r_{L6}}. \tag{3-6}$$

The IFAs of particle and chunk components are assigned to the bubbly and dispersed regions using the fractions defined later by Eqs. (3-22) and (3-23),

$$\left.\begin{aligned} A_{Lm,B} &= X_B A_{Lm} \\ A_{Lm,D} &= X_D A_{Lm} \end{aligned}\right\} \quad \text{for } m=4, 5, 6, 7\ . \tag{3-7}$$

3.2.2. Surface areas of structures

SIMMER-III has three structure surfaces, i.e. the fuel pin (*PIN*), the left can wall (*LC*) and the right can wall (*RC*). For SIMMER-IV, the front can wall (*FC*) and the back can wall (*BC*) are added. To make the liquid film not working as an energy shunt between these structure energy components if SIMMER-III is to possess only one energy component for a liquid material, the structure energy components are divided into "film" structure subscripted by *FS* and "vapor" structure subscripted by *VS*. The "film" structure is assumed to contact the liquid film while the "vapor" structure not. The allocation of each structure component to the "film" or "vapor" structure component is controlled by a parameter *ILS*. According to *ILS*, the "film" structure is defined as follows in SIMMER-III:

ILS = 1: *FS* = *PIN*
2: *FS* = *LC*
3: *FS* = *RC*
4: *FS* = *PIN and LC*
5: *FS* = *PIN and RC*
6: *FS* = *LC and RC*
7: *FS* = *PIN, LC, and RC*

and in SIMMER-IV:

ILS = 1: *FS* = *PIN*

2: *FS = Can walls*

3: *FS = All structures*

The default value of *ILS* is proposed to be 1. If a pin is not present or it breaks up, *ILS* should be changed appropriately based on phenomenological consideration. Currently, *ILS* is assumed to change according to the following algorithm in SIMMER-III:

(1) If a pin is not present when *ILS*=1, *ILS* becomes 2. In addition, if a left can wall is not present, *ILS* becomes 3.

(2) If a left can wall is not present when *ILS* =2, *ILS* becomes 1. In addition, if a pin is not present, *ILS* becomes 3.

(3) If a right can wall is not present when *ILS* =3, *ILS* becomes 1. In addition, if a pin is not present, *ILS* becomes 2.

(4) If a pin and a left can wall are not present when *ILS* =4, *ILS* becomes 2.

(5) If a pin and a right can wall are not present when *ILS* =5, *ILS* becomes 3.

(6) If left and right can walls are not present when *ILS* =6, *ILS* becomes 1.

(7) If no structure component exists, the code will calculate a pool flow.

In SIMMER-IV:

(1) If a pin is not present when *ILS*=1, *ILS* becomes 3.

(2) If can walls are not present when *ILS* =2, *ILS* becomes 3.

The surface areas of the “film” structure A_{FS} and the “vapor” structure A_{VS} are defined as follows, depending on the value of *ILS* in SIMMER-III.

$$A_{FS} = \begin{cases} A_{PIN} & : ILS = 1 \\ A_{LC} & : ILS = 2 \\ A_{RC} & : ILS = 3 \\ A_{PIN} + A_{LC} & : ILS = 4 \\ A_{PIN} + A_{RC} & : ILS = 5 \\ A_{LC} + A_{RC} & : ILS = 6 \\ A_{PIN} + A_{LC} + A_{RC} & : ILS = 7 \end{cases} \text{, and} \tag{3-8a}$$

$$A_{VS} = \begin{cases} A_{LC} + A_{RC} & : ILS = 1 \\ A_{PIN} + A_{RC} & : ILS = 2 \\ A_{PIN} + A_{LC} & : ILS = 3 \\ A_{RC} & : ILS = 4 \\ A_{LC} & : ILS = 5 \\ A_{PIN} & : ILS = 6 \\ 0 & : ILS = 7 \end{cases} . \quad (3\text{-}8b)$$

The definitions of the “film” structure and the “vapor” structure in SIMMER-IV becomes as follows.

$$A_{FS} = \begin{cases} A_{PIN} & : ILS = 1 \\ A_{LC} + A_{RC} + A_{FC} + A_{BC} & : ILS = 2 \\ A_{PIN} + A_{LC} + A_{RC} + A_{FC} + A_{BC} & : ILS = 3 \end{cases} \text{, and} \quad (3\text{-}9a)$$

$$A_{VS} = \begin{cases} A_{LC} + A_{RC} + A_{FC} + A_{BC} & : ILS = 1 \\ A_{PIN} & : ILS = 2 \\ 0 & : ILS = 3 \end{cases} . \quad (3\text{-}9b)$$

These surface areas are further divided into the bubbly and dispersed regions as follows:

$$A_{FS,B} = f_B A_{FS} , \quad (3\text{-}10)$$

$$A_{FS,D} = f_D A_{FS} , \quad (3\text{-}11)$$

$$A_{VS,B} = f_B A_{VS} \text{, and} \quad (3\text{-}12)$$

$$A_{VS,D} = f_D A_{VS} . \quad (3\text{-}13)$$

3.3. Pool Flow Topology

3.3.1. Pool flow regimes

The pool flow regime map modeled in SIMMER-III is depicted in Fig. 4. As already explained, three flow regimes are defined to cover an entire range of void fraction. The definitions of variables needed in this modeling are as follows.

α_S = Total structure volume fraction

$$\alpha_F = 1 - \alpha_S \quad (3\text{-}14)$$

= Volume fraction available for flow

$$\alpha_L = \alpha_{L1} + \alpha_{L2} + \alpha_{L3} \quad (3\text{-}15)$$

= Total real liquid volume fraction. Only the liquid fuel, steel, and sodium components are included in the summation and particles are excluded.

$$\alpha_P = \alpha_{L4} + \alpha_{L5} + \alpha_{L6} + \alpha_{L7} \tag{3-16}$$

= Total particle volume fraction

$$\alpha_G = 1 - \alpha_S - \alpha_L - \alpha_P \tag{3-17}$$

= Vapor volume fraction

$$\alpha = \frac{\alpha_G}{1 - \alpha_S - \alpha_P} \tag{3-18}$$

= (vapor volume)/(vapor volume + real liquid volume)

= Effective vapor volume fraction

$\alpha \leq \alpha_B$ describes the *bubbly* flow regime

$\alpha \geq \alpha_D$ describes the *dispersed* flow regime

$\alpha_B < \alpha < \alpha_D$ describes the *transition* regime

The volume fractions to describe the boundaries, α_B and α_D, are input constants. For the pool flow, a reasonable value of α_B is 0.3, whereas 0.7 appears appropriate for α_D. For the channel flow, 0.8 may be appropriate for α_D according to the experimental data.[14] The effective vapor fraction with limiting values is defined for use in the whole range of void fraction:

$$\alpha^* = \max[\alpha_B, \min(\alpha, \alpha_D)]\,. \tag{3-19}$$

The flow area is then divided into two parts:

$$f_B = \left\{1 + \frac{\alpha_P(\alpha^* - \alpha_B)}{\alpha_F(1 - \alpha^*)}\right\}\frac{(\alpha_D - \alpha^*)}{(\alpha_D - \alpha_B)} \tag{3-20}$$

= Volume fraction of liquid-continuous region,

and

$$f_D = \left\{1 - \frac{\alpha_P(\alpha_D - \alpha^*)}{\alpha_F(1 - \alpha^*)}\right\}\frac{(\alpha^* - \alpha_B)}{(\alpha_D - \alpha_B)} \tag{3-21}$$

= Volume fraction of vapor-continuous region.

The liquid components should be allocated to these two regions with the following fractions:

$$X_B = \frac{(1 - \alpha_B)}{(\alpha_D - \alpha_B)}\frac{(\alpha_D - \alpha^*)}{(1 - \alpha^*)} \tag{3-22}$$

= Fraction of Liquid components in liquid-continuous region, and

$$X_D = \frac{(1 - \alpha_D)}{(\alpha_D - \alpha_B)}\frac{(\alpha^* - \alpha_B)}{(1 - \alpha^*)} \tag{3-23}$$

= Fraction of Liquid components in vapor-continuous region.

These fractions are determined to satisfy the following two requirements. First the liquid-continuous (bubbly) region has a local effective vapor volume fraction of α_B and the dispersed region α_D. Second the

real liquids and particles should be partitioned between the two regions with the same fraction. The derivation of these fractions is described in Appendix A in detail.

Some additional definitions can be made using these fractions as follows.

$$\alpha_{F,B} = f_B \alpha_F \tag{3-24}$$

= Volume fraction available for flow in the liquid-continuous region

$$\alpha_{F,D} = f_D \alpha_F \tag{3-25}$$

= Volume fraction available for flow in the vapor-continuous region

$$\alpha_{Lm,B} = X_B \alpha_{Lm}\text{, for } m = 1 \sim 7 \tag{3-26}$$

= Volume fraction of liquid components in the liquid-continuous region

$$\alpha_{Lm,D} = X_D \alpha_{Lm}\text{, for } m = 1 \sim 7 \tag{3-27}$$

= Volume fraction of liquid components in the vapor-continuous region

$$\alpha_{G,B} = \begin{cases} \alpha_G & \text{for } \alpha < \alpha_B \\ \alpha_B[f_B(1-\alpha_S) - X_B\alpha_P] & \text{for } \alpha_B \le \alpha \end{cases} \tag{3-28}$$

= Volume fraction of vapor in the liquid-continuous region

$$\alpha_{G,D} = \begin{cases} \alpha_B[f_D(1-\alpha_S) - X_D\alpha_P] & \text{for } \alpha \le \alpha_D \\ \alpha_G & \text{for } \alpha_D < \alpha \end{cases} \tag{3-29}$$

= Volume fraction of vapor in the vapor-continuous region

3.3.2. Continuous liquid phase

The real liquid with the largest volume fraction is subscripted by *m*=*CP*. This liquid is assumed to form the continuous phase in the bubbly flow region. The convectible interfacial area of *CP* in the bubbly flow region is always set to be zero. To avoid oscillatory behavior resulting when *CP* changes on every other cycle, a hysteresis should be formulated. Thus, the change of *CP* does not occur unless the following condition is satisfied.

$$\alpha_{CP(old)} < C_{HTS}\max\{\alpha_{Lk}\}\text{,} \tag{3-30}$$

where *Lk* represents the other two real liquid components and C_{HTS} is a user defined constant less than unity. If this condition is satisfied, a new *CP* is defined using

$$\alpha_{CP(new)} = \max\{\alpha_{Lk}\}\text{.} \tag{3-31}$$

To conserve the interfacial area upon a *CP* switch, the convectible interfacial area of the new and old continuous phases in the bubbly flow region are exchanged by setting

$$A_{CP(old),B} = A_{CP(new),B}\text{, and} \tag{3-32}$$

$$A_{CP(new),B} = 0 . \quad (3\text{-}33)$$

3.3.3. Second continuous liquid phase

An abrupt change of IFAs may occur when a continuous phase changes to other components. To ensure the smooth transition of *CP* in this situation, a real liquid that has the second largest volume fraction and belongs to a velocity field different from *CP* is defined as the second continuous phase *CP*2. In order not to introduce excessive complexity, the second continuous phase is calculated after all the convectible IFAs are updated. The bubbly flow region is subdivided into the *CP*-continuous region (subscripted *B*1) and the *CP*2-continuous region (subscripted by *B*2). The remaining real liquid is defined as the dispersed phase subscripted by *DP*.

Based on the procedure described in Appendix B, the bubbly flow region is subdivided into two parts. The *B*1 region has a local *CP*2 volume fraction of α_{B1} whereas the *B*2 region has a local *CP*2 volume fraction of α_{B2}., where α_{B1} and α_{B2} are user specified input with the default values of 0.3 and 0.7, respectively. The dispersed liquid components (*m* = *DP*, 4, 5, 6, 7) and the vapor component are assumed to distribute uniformly in the bubbly region.

The convectible interfacial area of component *CP*2 in the *CP*-continuous region is assumed to be proportional to the volume fraction as follows

$$A_{CP2,B1} = \frac{\alpha_{CP,B1}}{\alpha_{CP2,B}} A_{CP2,B} , \quad (3\text{-}34)$$

where $\alpha_{CP,B1}$ is the volume fraction of *CP* in the *CP*-continuous region, $\alpha_{CP2,B}$ is the volume fraction of *CP*2 in the bubbly flow region and $A_{CP2,B}$ is the volume fraction of *CP* in the bubbly flow region. The interfacial area between component *CP* and *CP*2 must be conserved. Hence the reasonable definition for the interfacial area of component *CP* in *CP*2-continuous region is

$$A_{CP2,B2} = A_{CP2,B} - A_{CP2,B1} . \quad (3\text{-}35)$$

The IFA between *CP*-continuous and *CP*2-continuous regions is assumed to be zero. The remaining IFAs of *CP* and *CP*2 are set to zero similar to $A_{CP,B}$. These are

$$A_{CP,B1} = 0 , \text{and} \quad (3\text{-}36)$$

$$A_{CP2,B2} = 0 . \quad (3\text{-}37)$$

The convectible areas of dispersed liquid components and the surface areas of structures in the bubbly flow region are divided into the *CP*-continuous and *CP*2-continuous regions using the fractions of *CP*-continuous (*B*1) region and *CP*2-continuous (*B*2) region, f_{B1} and f_{B2}, respectively.

$$A_{FS,B1} = f_{B1} A_{FS,B} , \quad (3\text{-}38)$$

$$A_{FS,B2} = f_{B2} A_{FS,B} \,, \tag{3-39}$$

$$A_{VS,B1} = f_{B1} A_{VS,B} \,, \tag{3-40}$$

$$A_{VS,B2} = f_{B2} A_{VS,B} \,, \tag{3-41}$$

$$A_{Lm,B1} = f_{B1} A_{Lm,B} \quad \text{for } m=DP, 4, 5, 6, 7 \tag{3-42}$$

$$A_{Lm,B2} = f_{B2} A_{Lm,B} \quad \text{for } m=DP, 4, 5, 6, 7. \tag{3-43}$$

3.4. Channel Flow Topology

3.4.1. Channel flow regime map

Nine flow regimes are defined for the channel flow topology in SIMMER-III. The geometrical description of the channel flow is shown in Fig. 5. The ordinate of Fig. 5 is a fractional amount of liquid entrainment and the abscissa is the effective vapor volume fraction as defined in the pool flow topology.

The time-dependent entrainment fraction E_r is introduced to avoid instabilities, which are anticipated if the definition of flow regime is based on instantaneous quantities such as velocities[15), 16)]. That is, the evolution of E_r is calculated based on the differential equation:

$$\frac{\partial E_r}{\partial t} = \frac{1}{\tau_{en}} (E_u - E_r) \,, \tag{3-44}$$

where E_u is the equilibrium entrainment fraction for given flow conditions, and

τ_{en} is the entrainment time constant.

E_u is the upper limit of the entrainment fraction. The proposed formalisms for E_r, τ_{en} and E_u are described in Appendix C.

The bubbly regime, the dispersed regime, and the pool-type transition regime are treated similarly to the pool flow. Thus, the new equations necessary for the channel flow are those which model the slug flow regime, the annular flow regime, the annular-dispersed flow regime, and the interpolated regime.

3.4.2. Slug flow regime

The slug flow regime occupies a part of the flow regime map where $\alpha_B < \alpha < \alpha_D$ and $E_r = 0$. The schematic picture for the slug flow regime is shown in Fig. 6.

The flow area is divided into two regions, namely “film” and “channel” regions. The “channel” region is further divided into “slug” region and “vapor” region. Some assumptions need to be made in modeling the topology of this regime. First, as the annular flow approached, the bubbles are assumed to cross the interface to the “vapor” volume and the volume fraction of bubbles is now assumed to be proportional to the fraction of liquid continuous fluid in the flow volume:

$$\frac{(\alpha_{Slug}+\alpha_{Film})}{(1-\alpha_S)}.$$

The bubble volume fraction is then given by

$$\alpha_{G,SF} \equiv \alpha_{G,B}\frac{(\alpha_{Slug}+\alpha_{Film})}{(1-\alpha_S)}, \tag{3-45}$$

where $\alpha_{G,B}$ is defined by Eq. (3-28).

Second, the amount of liquid in the "film" volume is assumed to be constant and the same as the value at the transition point to the annular flow:

$$(\alpha_L+\alpha_P)_{Film} \equiv 1-\alpha_D(1-\alpha_S-\alpha_P)-\alpha_S = (1-\alpha_S)(1-\alpha_D)-\alpha_D\alpha_P\,. \tag{3-46}$$

Using Eq. (3-45), the "vapor" volume fraction is obtained as

$$\alpha_{Vapor} = \alpha_G - \alpha_{G,SF} = 1-\alpha_S-\alpha_{Film}-\alpha_{Slug}\,. \tag{3-47}$$

From Eqs. (3-46) and (3-47), we obtain

$$\alpha_{Film}+\alpha_{Slug} = \frac{1-\alpha_S-\alpha_G}{1-\alpha_S-\alpha_{G,B}}(1-\alpha_S)\,. \tag{3-48}$$

The "film" volume fraction is the sum of the bubble volume in the film and the film volume at $\alpha=\alpha_D$.

$$\alpha_{Film} = \alpha_{G,SF}\frac{\alpha_{Film}}{\alpha_{Film}+\alpha_{Slug}} + (\alpha_L+\alpha_P)_{Film} = \alpha_{G,SF}\frac{\alpha_{Film}}{1-\alpha_S} + (\alpha_L+\alpha_P)_{Film}\,. \tag{3-49}$$

Algebraic manipulation of Eq. (3-49) yields

$$\alpha_{Film} = \frac{(\alpha_L+\alpha_P)_{Film}}{1-\alpha_S-\alpha_{G,B}}(1-\alpha_S)\,. \tag{3-50}$$

The "channel" volume is defined by

$$\alpha_{Channel} \equiv \alpha_{Slug}+\alpha_{Vapor} = 1-\alpha_S-\alpha_{Film} = (1-\alpha_S)\frac{\alpha_D(1-\alpha_S-\alpha_P)-\alpha_{G,\boldsymbol{B}}}{1-\alpha_S-\alpha_{G,B}}. \tag{3-51}$$

The "slug" volume is obtained by substituting Eq. (3-51) to Eq. (3-48) as

$$\alpha_{Slug} = (1-\alpha_S)\frac{\alpha_D(1-\alpha_S-\alpha_P)-\alpha_G}{1-\alpha_S-\alpha_{G,B}}. \tag{3-52}$$

Geometrical variables are defined using these volume fractions as follows.

$$X_D = 0\,, \tag{3-53}$$

$$X_B = 1\,, \tag{3-54}$$

$$\alpha_{F,B} = \alpha_{Film}+\alpha_{Slug}\,, \tag{3-55}$$

$$\alpha_{F,D} = \alpha_{Vapor}\,, \tag{3-56}$$

$$f_B = \frac{\alpha_{F,B}}{(1-\alpha_S)}, \tag{3-57}$$

$$f_D = 1 - f_B\,, \tag{3-58}$$

$$\left.\begin{aligned}\alpha_{Lm,B} &= \alpha_{Lm}\\ \alpha_{Lm,D} &= 0\end{aligned}\right\} \text{ for } m{=}1 \sim 7\,, \tag{3-59}$$

$$\alpha_{G,B} = \alpha_{G,SF}\,, \tag{3-60}$$

$$\alpha_{G,D} = \alpha_{Vapor}\,, \tag{3-61}$$

$$\left.\begin{aligned}A_{Lm,B} &= A_{Lm}\\ A_{Lm,D} &= 0\end{aligned}\right\} \text{ for } m{=}4,5,6,7\,, \tag{3-62}$$

$$A_{FS,B} = A_{FS}\,, \tag{3-63}$$

$$A_{FS,D} = 0\,, \tag{3-64}$$

$$A_{VS,B} = \frac{\alpha_{Slug}}{\alpha_{Channel}} A_{VS}\,, \text{and} \tag{3-65}$$

$$A_{VS,D} = A_{VS} - A_{VS,B}\,. \tag{3-66}$$

Note that $\alpha_{G,B}$ is now re-defined by Eq. (3-60).

3.4.3. Annular flow regime

The annular flow regime occupies the part of the flow regime map where $\alpha_D \leq \alpha$ and $E_r = 0$. The conceptual picture for the annular flow regime is shown in Fig. 7.

The mixture of liquid components forms a liquid film on the structure and only the vapor occupies the remaining flow channel. Because the annular flow is considered as a limiting case of slug flow with no “slug” or vapor bubbles in the liquid-continuous region, the geometrical description is obtained by simplifying Eqs. (3-53) to Eq. (3-66). The geometrical variables are:

$$X_D = 0\,, \tag{3-67}$$

$$X_B = 1\,, \tag{3-68}$$

$$\alpha_{F,B} = \alpha_L + \alpha_P\,, \tag{3-69}$$

$$\alpha_{F,D} = 1 - \alpha_S - \alpha_{F,B}\,, \tag{3-70}$$

$$f_B = \frac{\alpha_{F,B}}{1-\alpha_S}, \tag{3-71}$$

$$f_D = 1 - f_B\,, \tag{3-72}$$

$$\left.\begin{aligned}\alpha_{Lm,B} &= \alpha_{Lm}\\ \alpha_{Lm,D} &= 0\end{aligned}\right\} \quad \text{for } m{=}1 \sim 7\,, \tag{3-73}$$

$$\alpha_{G,B} = 0\,, \tag{3-74}$$

$$\alpha_{G,D} = \alpha_G\,, \tag{3-75}$$

$$\left.\begin{aligned}A_{Lm,B} &= A_{Lm}\\ A_{Lm,D} &= 0\end{aligned}\right\} \quad \text{for } m{=}4,5,6,7\,, \tag{3-76}$$

$$A_{FS,B} = A_{FS}\,, \tag{3-77}$$

$$A_{FS,D} = 0\,, \tag{3-78}$$

$$A_{VS,B} = 0\,, \text{and} \tag{3-79}$$

$$A_{VS,D} = A_{VS}\,. \tag{3-80}$$

3.4.4. Annular-dispersed flow regime

The annular-dispersed flow regime is characterized by the film interface becoming unstable due to the velocity difference between vapor and liquid film. When the flooding criterion is met, liquid momentum coupling with the vapor increases by an order of magnitude. As the available pressure drop and velocities increase, the dispersed flow is achieved. This regime occupies the part of the flow regime map where $\alpha_D \leq \alpha$ and $0 < E_r \leq E_u$. The schematic picture for the annular-dispersed flow is shown in Fig. 8. This picture shows wavy liquid film and entrained liquid droplets in the dispersed region.

Some definitions required to treat the annular-dispersed region are:

$$X_D = \frac{E_r}{E_u} \tag{3-81}$$

= the fraction of liquid that is treated as the dispersed droplets,

$$X_B = 1 - X_D \tag{3-82}$$

= the fraction of liquid that is treated as the liquid film,

$$f_S = {X_B}^{C_{Sf}} \tag{3-83}$$

= the fraction of structure area still in film flow, and

$$\alpha_{F,B} = (\alpha_L + \alpha_P)X_B \tag{3-84}$$

= the volume fraction remaining in the structure film.

The remaining geometrical description can be obtained by the above definitions as follows:

$$\alpha_{F,D} = 1 - \alpha_S - \alpha_{F,B} \ , \tag{3-85}$$

$$f_B = \frac{\alpha_{F,B}}{(1-\alpha_S)} , \tag{3-86}$$

$$f_D = 1 - f_B \ , \tag{3-87}$$

$$\left.\begin{aligned} \alpha_{Lm,B} &= X_D \alpha_{Lm} \\ \alpha_{Lm,D} &= X_B \alpha_{Lm} \end{aligned}\right\} \quad \text{for } m=1 \sim 7 \ , \tag{3-88}$$

$$\alpha_{G,B} = 0 \ , \tag{3-89}$$

$$\alpha_{G,D} = \alpha_G \ , \tag{3-90}$$

$$\left.\begin{aligned} A_{Lm,B} &= X_B \alpha_{Lm} \\ A_{Lm,D} &= X_D \alpha_{Lm} \end{aligned}\right\} \quad \text{for } m=4, 5, 6, 7 \ , \tag{3-91}$$

$$A_{FS,B} = f_S A_{FS} \ , \tag{3-92}$$

$$A_{FS,D} = (1 - f_S) A_{FS} \ , \tag{3-93}$$

$$A_{VS,B} = 0 \ , \text{and} \tag{3-94}$$

$$A_{VS,D} = A_{VS} \ . \tag{3-95}$$

3.4.5. Interpolated regime

This flow regime occupies the part of the flow regime map where $\alpha_B < \alpha < \alpha_D$ and $0 < E_r \leq E_u$. IFA modeling is a formulation of the geometrical relations among the fluid components under given volume fractions and flow conditions. If we are to interpolate variables between the two limiting flow regimes which have different void fractions, we need to define the geometrical configuration of the flow similarly to the slug flow or the pool transition flow. Because of the difficulty in obtaining a geometrical configuration for this regime, a pure mathematical interpolation between the slug flow and the pool transition flow is performed.

The weighting fractions to interpolate between the two regimes are defined as

$$X_T = \frac{E_r}{E_u} \ , \text{and} \tag{3-96}$$

$$X_S = 1 - X_T \ . \tag{3-97}$$

Geometrical quantities are interpolated using these fractions. The quantities used in the right-hand side of the following equations are the same as defined for the pool transition flow model or the slug flow model.

$$\alpha_{F,B} = X_S\left(\alpha_{Film} + \alpha_{Slug}\right) + X_T f_{B,Pool}\alpha_F \,, \tag{3-98}$$

$$\alpha_{FD} = \alpha_F - \alpha_{F,B} \,, \tag{3-99}$$

$$\left.\begin{aligned}\alpha_{Lm,B} &= (X_S + X_T X_B)\alpha_{Lm} \\ \alpha_{Lm,D} &= X_T X_D \alpha_{Lm}\end{aligned}\right\} \quad \text{for } m\text{=}1 \sim 7 \,, \tag{3-100}$$

$$\alpha_{G,B} = X_S\alpha_{G,SF} + X_T\alpha_B\left[f_{B,Pool}(1-\alpha_S) - X_S\alpha_P\right], \tag{3-101}$$

$$\alpha_{G,D} = \alpha_{G-}\alpha_{G,B} \,, \tag{3-102}$$

$$\left.\begin{aligned}A_{Lm,B} &= (X_S + X_T X_B)A_{Lm} \\ A_{Lm,D} &= X_T X_D A_{Lm}\end{aligned}\right\} \quad \text{for } m\text{=}4, 5, 6, 7 \,, \tag{3-103}$$

$$A_{FS,B} = \left(X_S + X_T f_{B,Pool}\right)A_{FS} \,, \tag{3-104}$$

$$A_{FS,D} = X_T f_{D,Pool} A_{FS} \,, \tag{3-105}$$

$$A_{VS,B} = \left(X_S\frac{\alpha_{Slug}}{\alpha_{Channel}} + X_T f_{B,Pool}\right)A_{VS} \,, \text{and} \tag{3-106}$$

$$A_{VS,D} = \left[X_S\left(1 - \frac{\alpha_{Slug}}{\alpha_{Channel}}\right) + X_T f_{D,Pool}\right]A_{VS} \,. \tag{3-107}$$

Finally, the geometrical fractions used in Eqs. (3-96) to (3-107) are re-defined to keep consistency with the interpolated quantities as follows,

$$X_B = X_S + X_T\frac{(1-\alpha_B)(\alpha_D - \alpha^*)}{(\alpha_D - \alpha_B)(1-\alpha^*)}, \tag{3-108}$$

$$X_D = 1 - X_B \,, \tag{3-109}$$

$$f_D = \frac{\alpha_{F,B}}{1-\alpha_S} \,, \text{and} \tag{3-110}$$

$$f_D = 1 - f_B \,. \tag{3-111}$$

4. Convection of Interfacial Areas

4.1. Interfacial Area Convection Equation

In predicting the multi-component multi-phase thermohydraulic transients, the IFAs between components play very important roles in determining the rates of heat and mass transfer as well as momentum exchange. Although IFAs cannot be conserved in principle, a convection equation of an IFA per unit volume (IFA concentration) is proposed by Ishii[13] in a general form:

$$\frac{\partial A_i}{\partial t} + \nabla \cdot \left(\vec{v}_{q(i)} A_i\right) = \sum_k S_{i,k} \,, \tag{4-1}$$

where A_i is the convectible IFA per unit volume of interface *i*,

$\vec{v}_{q(i)}$ is the velocity of interface *i*, and

$S_{i,k}$ are the IFA source terms, which update the area of the interface *i*.

A total of 11 convectible IFAs per unit volume defined in SIMMER-III was already introduced in Section 3.1.1. The changes of IFAs resulting from breakup, coalescence, and production of droplets or bubbles are treated as “source term” of IFAs in the convection equations. This treatment seems to be appropriate, because: (a) the model is reasonably simple and concise with acceptable compromises in treating extremely complex flow configuration in SIMMER-III; (b) smooth changes of physical properties of the flow are guaranteed, such as IFAs and momentum exchange functions; and (c) current knowledge and technology about multi-component multi-phase flows are limited, so that more detailed modeling is not necessarily useful.

The additional terms are necessary to the above basic equation in order to calculate the IFA correctly under the complex multi-phase flow situation to which SIMMER-III is applied. In the rest of this chapter, the derivation of these additional terms will be discussed in detail.

4.2. Migration of IFA between Bubbly and Dispersed Flow Regions

In the present formulation of SIMMER-III, the IFAs of real liquids are treated separately in the bubbly and dispersed regions to take into accounts the difference of magnitude of the droplet radius between the two regions. The volume fraction of each component is also divided into the two regions, while the dividing fractions, X_B and X_D, are determined by the local volume fractions alone. When one field with two regions convects along the volume fraction gradient, the convectible IFAs must move through the boundary between the bubbly and dispersed regions. This diffusion or transfer process, called a “migration” process in general, is formulated in this section. There exist other migration mechanisms for IFAs due to physical phenomena such as bubble migration or droplet entrainment/deposition. However, these mechanisms should be treated in the source term modeling.

4.2.1. Formulation of migration terms

If the mass conservation equations are written for the bubbly and dispersed regions, the equations respectively will become

$$\frac{\partial \bar{\rho}_{M,B}}{\partial t} + \nabla \cdot \left(\vec{v}_{q(f)} \bar{\rho}_{M,B}\right) = \Gamma_{M,B} - \bar{\rho}_{M,B\to D} \text{ , and} \tag{4-2}$$

$$\frac{\partial \bar{\rho}_{M,D}}{\partial t} + \nabla \cdot \left(\vec{v}_{q(f)} \bar{\rho}_{M,D}\right) = \Gamma_{M,D} + \bar{\rho}_{M,B\to D} \text{ ,} \tag{4-3}$$

where $\bar{\rho}_M$ is the macroscopic density of component M

Γ_M is the mass transfer rate of component M

$\bar{\rho}_{M,B\to D}$ is the transfer rate of macroscopic density from the bubbly region to the dispersed region, and

subscripts B and D denote the values in the bubbly and the dispersed regions, respectively.

For the sake of simplicity of manipulation, the following operator is used hereinafter.

$$\chi(s) \equiv \frac{\partial s}{\partial t} + \nabla \cdot (\vec{v} s) \text{ .} \tag{4-4}$$

The following relationships hold for $\chi(s)$.

$$\chi(cs) = c\chi(s) \text{ ,} \tag{4-5}$$

$$\chi(\mathrm{s}_1 + \mathrm{s}_2) = \chi(\mathrm{s}_1) + \chi(\mathrm{s}_2) \text{ ,} \tag{4-6}$$

$$\chi(\mathrm{s}_1 \mathrm{s}_2) = \mathrm{s}_1 \chi(\mathrm{s}_2) + \mathrm{s}_2 \chi(\mathrm{s}_1) + \mathrm{s}_1 \mathrm{s}_2 \chi(1) \text{ , and} \tag{4-7}$$

$$\chi(s^n) = n s^{n-1} \chi(s) + (n-1)\chi(1) \text{ ,} \tag{4-8}$$

where, $\bar{\rho}_{M,B}$ and $\Gamma_{M,B}$ are assumed to be defined using a fraction ζ_B as follows,

$$\bar{\rho}_{M,B} = \zeta_B \bar{\rho}_M \text{ , and} \tag{4-9}$$

$$\Gamma_{M,B} = \zeta_B \Gamma_M \text{ .} \tag{4-10}$$

Substituting Eqs. (4-9) and (4-10) into Eq. (4-2) and rearranging, we obtain

$$\bar{\rho}_{M,B\to D} = \zeta_B \left(\Gamma_M - \chi(\bar{\rho}_M)\right) - \bar{\rho}_M \chi(\zeta_B) + \bar{\rho}_M \zeta_B \chi(1) \text{ .} \tag{4-11}$$

The first term on the right-hand side of Eq. (4-11) is zero from mass conservation. Consequently, $\bar{\rho}_{M,B\to D}$ is expressed as

$$\bar{\rho}_{M,B\to D} = -\bar{\rho}_M \chi(\zeta_B) + \bar{\rho}_M \zeta_B \chi(1) \text{ .} \tag{4-12}$$

Assuming that a convectible area associates to the macroscopic density of the corresponding energy component, the migration rate of IFA from the bubbly to the dispersed region, $A_{M,B\to D}$, is obtained from

$$\begin{aligned} A_{M,B\to D} = \bar{\rho}_{M,B\to D} \frac{A_{M,B}}{\bar{\rho}_{M,B}} &= -\frac{A_{M,B}}{\zeta_B}\left[\chi(\zeta_B) - \zeta_B \chi(1)\right] = -\frac{A_{M,B}}{\alpha_{M,B}}\left[\frac{\alpha_{M,B}}{\zeta_B}\chi(\zeta_B) - \alpha_{M,B}\chi(1)\right] \\ &= -\frac{A_{M,B}}{\alpha_{M,B}}\left[\chi\left(\alpha_{M,B}\right) - \zeta_B \chi(\alpha_M)\right] \\ &= -\frac{A_{M,B}}{\alpha_{M,B}}\left[\alpha_M \frac{\partial \zeta_B}{\partial t} + \nabla \cdot \left(\vec{v}\alpha_{M,B}\right) - \zeta_B \nabla \cdot (\vec{v}\alpha_M)\right], \end{aligned} \tag{4-13}$$

for $\bar{\rho}_{M,B\to D} \geq 0$. Similarly,

$$A_{M,B\to D} = \frac{A_{M,B}}{\alpha_{M,B}}\left[\alpha_M \frac{\partial \zeta_D}{\partial t} + \nabla\cdot\left(\vec{v}\alpha_{M,D}\right) - \zeta_D \nabla\cdot\left(\vec{v}\alpha_M\right)\right], \tag{4-14}$$

for $\bar{\rho}_{M,B\to D} < 0$, where $\zeta_D = 1 - \zeta_B$.

Using $A_{M,B\to D}$, the convection equations of $A_{M,B}$ and $A_{M,D}$ are written as

$$\frac{\partial A_{M,B}}{\partial t} + \nabla\cdot\left(\vec{v}A_{M,B}\right) = \sum_k S_{M,B,k} - A_{M,B\to D} \text{ , and} \tag{4-15}$$

$$\frac{\partial A_{M,D}}{\partial t} + \nabla\cdot\left(\vec{v}A_{M,D}\right) = \sum_k S_{M,D,k} + A_{M,B\to D} \text{ .} \tag{4-16}$$

The fraction ζ_B is

$$\zeta_B = X_B \quad \text{for the liquid components } (M{=}Lm), \text{ and} \tag{4-17}$$

$$\zeta_B = \frac{\alpha_{G.B}}{\alpha_G} \quad \text{for the vapor } (M{=}G). \tag{4-18}$$

4.2.2. Implementation of migration terms

In the implementation of the migration terms Eq. (4-13) and Eq. (4-14), donor-cell differencing is used in the view point of the consistency with the fluid convection differencing scheme. Here, the notation "~n" means the value just after the heat and mass transfer calculation, and the notation "~n+1" means the value just after the calculation of convection. Eq. (4-13) is finite-differenced as

$$\begin{aligned} A_{M,B\to D} &= -\frac{\tilde{A}^n{}_{M,B}}{\alpha_{M,B}}\left[\frac{\alpha_{M,B}}{\zeta_B}\chi(\zeta_B) - \alpha_{M,B}\chi(1)\right] = -\frac{A_{M,B}}{\alpha_{M,B}}\left[\chi\left(\alpha_{M,B}\right) - \zeta_B\chi(\alpha_M)\right] \\ &= -\frac{A_{M,B}}{\alpha_{M,B}}\left[\alpha_M\frac{\partial\zeta_B}{\partial t} + \nabla\cdot\left(\vec{v}\alpha_{M,B}\right) - \zeta_B\nabla\cdot\left(\vec{v}\alpha_M\right)\right]. \end{aligned} \tag{4-19}$$

4.3. Compression of Fluid

Equation (4-1) has a difficulty in predicting the changes of IFAs due to the expansion or compression of fluid components without their convection. This difficulty is pronounced for the IFA of bubbles. Let us consider the situation in which a stagnant bubble is compressed rapidly by the liquid in-flow as shown in Fig. 9.

The bubble shrinks due to the liquid in-flow and then the surface area of the bubble decreases in proportion to the 2/3-rd power of the bubble volume, but this change cannot be predicted by Eq. (4-1). A possible remedy to this problem is to include the source term due to this mode of volume change. An attempt was made in AFDM by updating the IFA by the following formula that takes into account the IFA change due to mass transfer:

$$A_G^{n+1} = A_G^n \frac{3}{r}(\alpha_G^{n+1} - \alpha_G^n)\,, \tag{4-20}$$

where A_G^n and α_G^n are the current IFA of bubbles and void fraction, respectively,
A_G^{n+1} and α_G^{n+1} are the updated IFA of bubbles and void fraction, respectively, and
r is the bubble radius.

SIMMER-III uses a similar but improved expression:

$$A_G^{n+1} = A_G^n \left(\frac{\alpha_G^{n+1}}{\alpha_G^n}\right)^{\frac{2}{3}}. \tag{4-21}$$

These remedies are applicable to the volume change due to mass transfer, but they do not necessarily help the problem, in such a situation that a volume change of bubbles occurs only by the liquid convection and the resultant bubble compression. The difficulty originates from the fact that we use Eq. (4-1) to follow the space and time dependent change of IFA, actually IFA is not a conservative quantity. Instead of the IFA per unit volume, the number density of bubbles is thought to be conserved through the convection.

$$\frac{\partial n_i}{\partial t} + \nabla \cdot \left(\vec{v}_{q(i)} n_i\right) = \sum_k S_{n,i,k}\,, \tag{4-22}$$

where n_i is the number density of component *i*,
$\vec{v}_{q(i)}$ is the velocity of component *i*, and
$\vec{v}_{q(i)}$ are the source terms of number density of component *i*.

Assuming the spherical shape for droplets and/or bubbles, the number density is related to the surface area A_i and volume fraction α_i by the following equation:

$$n_i = \frac{{A_i}^3}{36\pi {\alpha_i}^2}. \tag{4-23}$$

In the case of ellipsoidal shape, the constant 36 for sphere may be different but the functional form does not change. Substituting Eq. (4-23) into Eq. (4-22) and rearranging, we get the following equation for the convection of IFA.

$$\chi(A_i) - \frac{2A_i}{3\alpha_i}\chi(\alpha_i) = 12\pi \frac{{\alpha_i}^2}{{A_i}^2} \sum_k S_{n,i,k}\,. \tag{4-24}$$

This is the IFA convection equation for the compressible fluid. The second term on the left-hand side takes into account the effect of the change in specific volume. This term was implemented in SIMMER-III and was validated by sample calculations, as detailed in Appendix D.

4.4. Discussion on Migrating IFA of Continuous Phase

As discussed in Section 4.1, the migration of components is considered across the boundary of bubbly and dispersed flow regions according to the void fraction change due to phase change and convection. The migration term of IFA of dispersed phase, such as droplets and bubbles, is clearly defined by Eq. (4-13) or

Eq. (4-14). However, the IFA migration terms of continuous phase, $A_{CP,B\to D}$ and $A_{G,B\to D}$ still remain to be defined, even when $A_{CP,B} = A_{G,B} = 0$, to keep the smooth change of total IFA under transient conditions.

Let us consider the flow situation in Edward's two-phase blowdown experiment shown in Fig. 10. The void fraction at the location "A" and "B" are 30% and 50%, respectively. As time goes on, the flow situation at "A" will become similar to "B" due to the increase in void fraction by flashing of water. The flow regime at the location "B" is foamy flow, in which the bubbles generated by vaporization occupy the flow area as shown in this figure. On the other hand, the flow regime model of SIMMER-III implies that the local void fraction in bubbly flow region is kept to $\alpha_B = 0.3$ and hence some fraction of continuous liquid and bubble is transferred to dispersed flow region. To keep the total IFA in the flow area, the newly created droplets should have appropriate IFA. This is realized by assigning the following IFA to $A_{CP,B\to D}$ in this case.

$$A_{CP,B\to D} = \alpha_{CP,B\to D}\frac{A_{G,B}}{\alpha_{G,B}}. \tag{4-25}$$

However, this formulation may cause numerical problem upon transition from the transition flow regime to dispersed flow regime. At this transition, the volume fraction of bubbly flow region f_B is very small but the surface area of bubble per unit volume of bubble $A_{G,B}/\alpha_{G,B}$ can be very large due to the large velocity difference between gas and liquid. This produces unrealistically large $A_{CP,B\to D}$ and results in a numerical instability. To mitigate this problem, a remedy is introduced to multiply Eq. (4-25) by the volume fraction of the bubbly flow regime f_B as follows.

$$A_{CP,B\to D} = \alpha_{CP,B\to D}\frac{A_{G,B}}{\alpha_{G,B}}f_B\,. \tag{4-26}$$

These formulations are optionalized by input parameter IFAOPT(3) for inter-cell convection and IFAOPT(6) for intra-cell phase change. The default model uses Eq. (4-26). The same formulation is provided for the IFA of bubble as,

$$A_{G,D\to B} = \alpha_{G,D\to B}\frac{A_{CP,B}}{\alpha_{CP,B}}, \tag{4-27}$$

which corresponds to Eq. (4-25), and

$$A_{G,D\to B} = \alpha_{G,D\to B}\frac{A_{CP,B}}{\alpha_{CP,B}}f_D\,, \tag{4-28}$$

which corresponds to Eq. (4-26). These are also optionalized by input parameters IFAOPT(4) and IFAOPT(7). The default model option uses Eq. (4-28).

4.5. Solution Procedure

The same differencing scheme as the fluid convection should be used for the sake of consistency. The notation "~" means the value just after the heat and mass transfer calculation, and the notation "~n+1" means the value just after the calculation of convection. Equation (4-13) is finite-differenced by the first-order donor-cell differencing in two dimensions for SIMMER-III.:

$$A_{M,D\to B} = -\left[\frac{\tilde{A}^n_{M,B\,i,j}}{\tilde{\zeta}^n_{B\,i,j}}\left(\frac{\tilde{\zeta}^{n+1}_{B\,i,j} - \tilde{\zeta}^n_{B\,i,j}}{\Delta t}\right) + \frac{\Delta_i\langle r^\rho \tilde{u}^{n+1}_q \tilde{A}^n_{M,B}\rangle_j}{r^\rho \Delta r_i} + \frac{\Delta_j\langle \tilde{v}^{n+1}_q \tilde{A}^n_{M,B}\rangle_i}{\Delta z_j} - \tilde{\zeta}^n_{B\,i,j}\left\{\frac{\Delta_i\langle r^\rho \tilde{u}^{n+1}_q \frac{\tilde{A}^n_{M,B}}{\tilde{\zeta}^n_B}\rangle_j}{r^\rho \Delta r_i} + \frac{\Delta_j\langle \tilde{v}^{n+1}_q \frac{\tilde{A}^n_{M,B}}{\tilde{\zeta}^n_B}\rangle_i}{\Delta z_j}\right\}\right], \tag{4-29}$$

where

$$\Delta_i\langle f\rangle_j = \langle f\rangle_{i+\frac{1}{2},j} - \langle f\rangle_{1-\frac{1}{2},j}, \tag{4-30}$$

$$\Delta_j\langle f\rangle_i = \langle f\rangle_{i,j+\frac{1}{2}} - \langle f\rangle_{1,j-\frac{1}{2}}, \tag{4-31}$$

$$\langle \tilde{v}^{n+1}_q \tilde{A}^n_{M,B}\rangle_{i,j+\frac{1}{2}} = \tilde{v}^{n+1}_{q\,i,j+\frac{1}{2}}\left[\mathrm{H}\left(\tilde{v}^{n+1}_{q\,i,j+\frac{1}{2}}\right)\tilde{A}^n_{M,B\,i,j} + \mathrm{H}\left(-\tilde{v}^{n+1}_{q\,i,j+\frac{1}{2}}\right)\tilde{A}^n_{M,B\,i,j+1}\right], \tag{4-32}$$

$$\langle \tilde{v}^{n+1}_q \frac{\tilde{A}^n_{M,B}}{\tilde{\zeta}^n_B}\rangle_{i,j+\frac{1}{2}} = \tilde{v}^{n+1}_{q\,i,j+\frac{1}{2}}\left[\mathrm{H}\left(\tilde{v}^{n+1}_{q\,i,j+\frac{1}{2}}\right)\frac{\tilde{A}^n_{M,B\,i,j}}{\tilde{\zeta}^n_{B\,i,j}} + \mathrm{H}\left(-\tilde{v}^{n+1}_{q\,i,j+\frac{1}{2}}\right)\frac{\tilde{A}^n_{M,B\,i,j+1}}{\tilde{\zeta}^n_{B\,i,j+1}}\right], \tag{4-33}$$

$$\begin{aligned}\langle r^\rho \tilde{u}^{n+1}_q \tilde{A}^n_{M,B}\rangle_{i+\frac{1}{2},j} &= r^\rho_{\,i+\frac{1}{2},j}\tilde{u}^{n+1}_{q\,i+\frac{1}{2},j}\left[\mathrm{H}\left(\tilde{u}^{n+1}_{q\,i+\frac{1}{2},j}\right)\tilde{A}^n_{M,B\,i,j}\right. \\ &\left. + \mathrm{H}\left(-\tilde{u}^{n+1}_{q\,i+\frac{1}{2},j}\right)\tilde{A}^n_{M,B\,i+1,j}\right], \text{and}\end{aligned} \tag{4-34}$$

$$\begin{aligned}\langle r^\rho \tilde{u}^{n+1}_q \frac{\tilde{A}^n_{M,B}}{\tilde{\zeta}^n_B}\rangle_{i+\frac{1}{2},j} &= r^\rho_{\,i+\frac{1}{2},j}\tilde{u}^{n+1}_{q\,i+\frac{1}{2},j}\left[\mathrm{H}\left(\tilde{u}^{n+1}_{q\,i+\frac{1}{2},j}\right)\frac{\tilde{A}^n_{M,B\,i,j}}{\tilde{\zeta}^n_{B\,i,j}}\right. \\ &\left. + \mathrm{H}\left(-\tilde{u}^{n+1}_{q\,i+\frac{1}{2},j}\right)\frac{\tilde{A}^n_{M,B\,i+1,j}}{\tilde{\zeta}^n_{B\,i+1,j}}\right].\end{aligned} \tag{4-35}$$

Equation (4-14) is also finite-differenced as:

$$A_{M,B\to D} = \frac{\tilde{A}^n_{M,D\,i,j}}{\tilde{\zeta}^n_{D\,i,j}}\left(\frac{\tilde{\zeta}^{n+1}_{D\,i,j} - \tilde{\zeta}^n_{D\,i,j}}{\Delta t}\right) + \frac{\Delta_i\langle r^\rho \tilde{u}^{n+1}_q \tilde{A}^n_{M,D}\rangle_j}{r^\rho \Delta r_i} + \frac{\Delta_j\langle \tilde{v}^{n+1}_q \tilde{A}^n_{M,D}\rangle_i}{\Delta z_j} - \tilde{\zeta}^n_{B\,i,j}\left\{\frac{\Delta_i\langle r^\rho \tilde{u}^{n+1}_q \frac{\tilde{A}^n_{M,D}}{\tilde{\zeta}^n_D}\rangle_j}{r^\rho \Delta r_i} + \frac{\Delta_j\langle \tilde{v}^{n+1}_q \frac{\tilde{A}^n_{M,D}}{\tilde{\zeta}^n_D}\rangle_i}{\Delta z_j}\right\}. \tag{4-36}$$

The finite-differencing for three-dimensional SIMMER-IV is formulated similarly to SIMMER-III and consistently with fluid convection.

A thought experiment may be useful to obtain some insight. Figure 11 illustrates the situation that $L2$ droplets in a dispersed regime cell flow into the neighboring bubbly regime cell filled with continuous phase $L1$. In this case, ∇X_B and $v_{q(L2)}$ are positive at the cell boundary (i, j+1/2). Consequently, $\bar{\rho}_{L2,B\to D}$ becomes negative in the cell (i, j) and IFA of $L2$ will be transferred from the dispersed region to the bubbly region in the cell (i, j). The transfer rate is calculated by Eq. (4-29) as

$$A_{L2,D\to B} = \frac{-v_{i,j-\frac{1}{2}} A_{L2,D\,i,j-1}}{\Delta z_j} - X_{D\,i,j} \frac{-v_{i,j-\frac{1}{2}} A_{L2,D\,i,j-1}}{\Delta z_j X_{D\,i,j-1}} = \frac{-v_{i,j-\frac{1}{2}} A_{L2,D\,i,j-1}}{\Delta z_j} . \tag{4-37}$$

In other words, $A_{L2,D}$ convected from cell (i,j-1) becomes $A_{L2,B}$ in the cell (i,j). This result seems reasonable.

5. Source Terms for Interfacial Areas

The convection equations for a convectible IFA can be written with the general form

$$\frac{\partial A_f}{\partial t} + \nabla \cdot \left(\vec{v}_{q(f)} A_f\right) = \sum_k S_{f,k} - A_{f,B\leftrightarrow D} \,, \tag{5-1}$$

where A_f is the convectible IFA per unit volume of the associating energy component *f*,

$\vec{v}_{q(f)}$ is the velocity of the energy component *f*,

$S_{f,k}$ are the IFA source terms, which update the IFA of the energy component *f.* and

$A_{f,B\leftrightarrow D}$ is the migration rate of A_f through the boundary of the bubbly and dispersed regions.

The source term model is classified into three types by their formulations. The first type of the source terms is modeled with an equilibrium value and a time constant:

$$S_k = \frac{A_{ek} - A_f}{\tau_k}, \tag{5-2}$$

where A_{ek} is the equilibrium value, and

τ_k is the time constant.

The second type of source terms is expressed with an exponent and a proportional constant:

$$S_i = -A_f^{\rho_l} \Gamma_i \,, \tag{5-3}$$

where ρ_l is the index, and

Γ_i is the proportional constant.

The third type of source terms is simply due to mass transfer or the change of microscopic density.

The IFA source terms are modeled separately for three situations of fluids: the bubbles in the bubbly flow, the droplets in the bubbly flow, and the droplets in the dispersed flow. This is because the combination of the physical properties and the flow configuration which dominate the source terms may differ significantly in different situations.

The formulae of source terms were developed in the precious AFDM code especially for the pool flow regime. Many of these are adopted for use in SIMMER-III with some adjustment to fit in the code framework. The source terms for the pool flow are discussed first in this chapter, followed by the channel flow, to which many of the source terms for the pool flow are applicable as well. The remaining topics for the channel flow will be discussed next.

5.1. Bubbles in Bubbly Region

For this situation, the convectible IFA is $A_{G,B}$. The source terms modeled are:

S_N : Bubble nucleation,

S_{WB} : Weber number breakup of bubbles,

S_{TB} : Turbulence breakup of bubbles,

S_{CB} : Coalescence of bubbles,

S_{MB} : Mass transfer to bubbles, and

S_{CV} : Volume change due to convection of other liquids.

In addition, a maximum $A_{G,B}$ based on a user-input minimum radius (default: 10^{-5} m) and a minimum $A_{G,B}$ based on Eotvos (Eö) number of 40, user-input maximum radius, and hydraulic diameter are proposed. The lower limit (minimum radius) of 10^{-5} m is generally sufficient to force rapid equilibration. The discontinuous phase with Eö >40 violates the multiphase continuity assumptions used to form the differential equations. Finally, the bubbles cannot become greater than the hydraulic radius of the cell. The treatments of each source term are given in the following sub-sections.

5.1.1. Nucleation

The source term is given by

$$S_{G,B,N} = \max\left(\frac{A^e_{G,B,N} - A_{G,B}}{\tau_N},\ 0\right), \tag{5-4}$$

where the equilibrium area is

$$A^e_{G,B,N} = (36\pi M_b)^{\frac{1}{3}}\left(\alpha_{G,B}\right)^{\frac{2}{3}}, \tag{5-5}$$

where M_b is the number of nucleation sites per unit volume.

There are two models implemented. The first and standard model based on AFDM gives M_b as follows. The liquid component with the largest dimensionless superheat is determined, assuming its nucleation should suppress bubbles of the other components to nucleate. The dimensionless superheat is defined by

$$\vartheta_{sup,Lm} = \frac{T_{Lm} - T_{sat}(P_{Gm})}{T_{crt,m}} - \frac{P_{crt,m}\mathrm{H}\left(\alpha_{Lm} - \alpha_N^t\right)}{\max\left[P_{crt,m} - P_{sat}(T_{Lm}),\ 10^{-20}\right]}, \tag{5-6}$$

where m=1, 2, 3 for three real liquids/vapor possibilities,

H(x) is the Heaviside function,

crt denotes the critical point,

sat denotes the saturation line, and

α_N^t is the minimum volume fraction to participate in bubble nucleation (default: 10^{-2}).

Then, m is determined as the liquid component having the largest superheat, ϑ_{Max},

$$\vartheta_{Max} = \max\left[0, \vartheta_{sup,L1},\ \vartheta_{sup,L2},\ \vartheta_{sup,L3}\right].$$

The nucleation site density is given by

$$M_b = \begin{cases} 0 & \text{for } \vartheta_0 \le 0 \\ M_{min} f_B (1-\alpha_S) & \text{for } \vartheta_{max} < \vartheta_0 \text{ and } P_{sat}(T_{Lm}) \le 0.9 P_{crt,m} \\ M_{min} + M_{max}[1-\exp(-C_\vartheta [\vartheta_{max} - \vartheta_0]^2)] & \text{for } \vartheta_{max} \ge \vartheta_0 \text{ and } P_{sat}(T_{Lm}) \le 0.9 P_{crt,m} \\ (M_{min} + M_{max})(1-\alpha_S) f_B & \text{for } P_{sat}(T_{Lm}) > 0.9 P_{crt,m} \end{cases}, \quad (5\text{-}7)$$

where ϑ_0 is the minimum superheat to participate in bubble nucleation (default: 2.0×10^{-3}),
M_{min} is the minimum nucleation site density (default: 10^5),
M_{max} is the maximum nucleation site density (default: 10^{11}), and
C_ϑ is user-input constant (default: 10^5).

The time constant is given by

$$\tau_N = \tau_{NUC} \exp\left(C_{NC} \frac{\max[0, \alpha - \alpha_{NC}]}{\max[\alpha_B - \alpha, 10^{-2}]} \right), \quad (5\text{-}8)$$

where τ_{NUC} is user-input (default: 10^{-4}), and α_{NC} is the effective void fraction above which bubble nucleation cannot occur (default: 0.1).

The second model based on Riznic and Ishii[17], for bubble generation in flashing flow, is optionally available (activated by IFAOPT(25)=1) and is used if $T_{Lm} > T_{sat.PG}$. In this model, the time constant and the equilibrium IFA are given by

$$\tau_N = \frac{1}{f_{DP}} \exp\left(\frac{C_{NC} \max[0, \alpha_{G,eff} - \alpha_{NC}]}{\max[0.01, \alpha_{NC} - \alpha_{G,eff}]} \right), \text{ and} \quad (5\text{-}9)$$

$$A^e_{G,B,N} = \begin{cases} 6\alpha_{G,B}/d_{DPX} & \text{for } T_{Lm} > T_{sat.PG} \\ 0 & \text{for } T_{Lm} \le T_{sat.PG} \end{cases}, \quad (5\text{-}10)$$

where f_{DP} is bubble departure frequency given by,

$$f_{DP} = \frac{1.18}{d_{DP}} \left(\frac{\sigma_{CP} g \Delta\rho}{{\rho_{CP}}^2} \right)^{0.25}, \quad (5\text{-}11)$$

and d_{DP} is bubble departure diameter given by

$$d_{DP} = 2.64 \times 10^{-5} C_{ANG} \sqrt{\frac{\sigma_{CP}}{g\Delta\rho}} {R_\rho}^{0.9}, \quad (5\text{-}12)$$

where σ_{CP} is the surface tension of continuous phase, C_{ANG} is the contact angle, and $\Delta\rho$ and R_ρ are defined as

$$\Delta\rho = \rho_{CP} - \rho_G, \text{ and} \quad (5\text{-}13)$$

$$R_\rho = \frac{\Delta\rho}{\rho_G}. \quad (5\text{-}14)$$

The effective nucleation density X_{NB} is given by

$$X_{NB} = \frac{2.157 \times 10^{-7} {R_\rho}^{-3.12} \left(1 + 0.0049 R_\rho\right)^{0.43}}{{d_{DP}}^2} \left(\frac{4\sigma_{CP} T_{sat,PG}}{d_{DP}(T_{Lm} - T_{sat.PG}) \rho_G h_{LG}} \right)^{-4.4}, \tag{5-15}$$

where h_{LG} is latent heat of vaporization, and. $T_{sat,PG}$ is saturation temperature. The bubble number density per unit volume M_b and the effective bubble radius d_{DPX} become

$$M_b = \frac{4 X_{NB} (1 - \alpha_S)}{D_H f_B} \text{ , and} \tag{5-16}$$

$$d_{DPX} = \max\left(d_{DP}, \left(\frac{6\alpha_{G,B}}{\pi M_b} \right)^{1/3} \right). \tag{5-17}$$

Note that the use of an equilibrium value and a time constant in Eq. (5-4) may not be appropriate for bubble nucleation, because IFA production due to actual bubble nucleation should result from vaporization mass transfer. If the rate of mass transfer due to boiling is correlated to vapor volume change, the bubble IFA can be updated by the following equation, which is obtained by differencing Eq. (5-5) with respect of time.

$$\frac{dA_{G,B,N}}{dt} = \left(\frac{36\pi M_b}{\alpha_{G,B}} \right)^{\frac{1}{3}} \frac{d\alpha_{G,B}}{dt}. \tag{5-18}$$

This equation is likely to underestimate the vapor-liquid IFAs and the mass-transfer rate upon boiling inception. Since there little information available to justify the use of Eq. (5-18), the standard model with Eq. (5-4) is simply used.

5.1.2. Weber number breakup of bubbles

The source term is given by

$$S_{G,B,WB} = \max\left(0, \frac{A^e_{G,B,WB} - A_{G,B}}{\tau_{G,B,WB}} \right), \tag{5-19}$$

where the equilibrium area is

$$A^e_{G,B,WB} = \frac{3\alpha_{G,B}}{r^e_{G,B,WB}}. \tag{5-20}$$

The equilibrium radius is obtained from a user-defined critical Weber number for bubbles We_B as

$$r^e_{G,B,WB} = \frac{\mathrm{We}_B \sigma_{CP}}{4\rho_{CL} \Delta v^2} + \sqrt{\left(\frac{\mathrm{We}_B \sigma_{CP}}{4\rho_{CL} \Delta v^2} \right)^2 + \frac{7}{2} C_{FV} \frac{{\mu_G}^2}{\rho_{CL} \rho_G \Delta v^2}}, \tag{5-21}$$

where C_{FV} is a user-defined multiplier of the viscous term (default: 10^{-4}), and
Δv is the velocity difference between the vapor ant continuous liquid component given by

$$\Delta v = \max\left(10^{-4}, \left| \vec{v}_{q(CP)} - \vec{v}_G \right| \right), \tag{5-22}$$

and ρ_{CL} is the microscopic density of a continuous phase,

$$\rho_{CL} = \begin{cases} \dfrac{\bar{\rho}_{L1}}{\alpha_{L1}} & \text{for } CP = 1 \\ \dfrac{(\bar{\rho}_{L2} + \bar{\rho}_{L2})}{(\alpha_{L2} + \alpha_{L3})} & \text{for } CP \neq 1 \end{cases}. \tag{5-23}$$

The time constant is given by

$$\tau_{G,B,WB} = 2\mathrm{C}_{FT} \frac{r_{G,B}}{\Delta v} \max\left(1,\ \frac{\Delta v}{\Delta v_{RT}}\right)\left(\frac{\rho_G}{\rho_{CL}}\right)^{\frac{1}{2}}, \tag{5-24}$$

where C_{FT} is a user-defined constant (default: 1.0), and Δv_{RT} is a user-defined velocity difference to accelerate the breakup at high velocity difference (default: 0.2 m/s).

5.1.3. Turbulence breakup of bubbles

The source term is given by

$$S_{G,B,TB} = \max\left(0,\ \frac{A^e_{G,B,TB} - A_{G,B}}{\tau_{G,B,TB}}\right). \tag{5-25}$$

A bubble can break up if its eigen-frequency corresponds to the frequency of the forces from turbulent eddies. This criterion for the lowest eigen frequency is given by

$$\tau_{e,TB} = \frac{2r_{G,B}}{\sqrt{v'v'}}, \tag{5-26}$$

where $v'v'$ is square of turbulence velocity, and the time constant is expressed as

$$r_{e,TB} = \frac{24}{31} \frac{2^{\frac{2}{3}}\sigma_{CP}}{3\rho_G + 2\rho_{CP}} \frac{1}{v'v'}. \tag{5-27}$$

Obtaining the quantity $v'v'$ is difficult, since the turbulent kinetic energy is not explicitly modeled in SIMMER-III. Thus, when the radial motion is possible, an analogy to Prandtl's mixing length hypothesis is used as follows.

$$v'v' = C_{TB} {r_{G,B}}^2 \left\{\left[\frac{\partial(u_G - u_{CP})}{\partial z}\right]^2 + \left[\frac{\partial(v_G - v_{CP})}{\partial r}\right]^2\right\}. \tag{5-28}$$

If the flow is restricted in a vertical channel, the turbulence breakup caused by buoyancy is modeled as follows.

$$v'v' = \frac{C_{RGB}\alpha_G}{1 - \alpha_S}\left(1 - \frac{\alpha_G}{1 - \alpha_S}\right)\left(1 - \frac{\rho_G}{\rho_{CP}}\right) g\,. \tag{5-29}$$

A larger of Eqs. (5-28) and (5-29) is used.

5.1.4. Bubble coalescence

The formula developed for SIMMER-II is used as:

$$\frac{d}{dt}r_{G,B} = \frac{\omega_B v'}{8f_B(1-\alpha_S)}, \tag{5-30}$$

where ω_B is coalescence probability per one collision, and

v' is mean velocity fluctuation of bubble.

The rate of IFA change can be deduced from this equation as follows

$$\frac{d}{dt}A_{G,B} = -\frac{3}{{r_{G,B}}^2}\frac{d}{dt}r_{G,B} = \frac{\omega_B {A_{G,B}}^2 v'}{24f_B(1-\alpha_S)}. \tag{5-31}$$

The velocity fluctuation v' is assumed such that $\sqrt{v'v'}$ from the turbulence modeling might be used as v' for bubbles, because the specific turbulent kinetic energy for vapor is unknown.

5.1.5. Mass transfer for bubbles

During the heat and mass transfer calculations, the volume fraction of each component may change as a result of mass transfer or temperature change. There are two cases with different update procedures. When the bubble nucleation is occurring, the IFA is updated by the finite-differenced form of Eq. (5-5) as

$$\tilde{A}_{G,B}^{n+1} - \tilde{A}_{G,B}^{n} = \left(\frac{36\pi M_b}{\alpha_{G,B}^{n}}\right)^{\frac{1}{3}} - \left(\tilde{\alpha}_{G,B}^{n+1} - \tilde{\alpha}_{G,B}^{n}\right), \text{ for } \alpha_{G,B} \le \alpha_{NC}. \tag{5-32}$$

Otherwise, the update equation is simply expressed by

$$\frac{\tilde{A}_{G,B}^{n+1}}{\tilde{A}_{G,B}^{n}} = \left(\frac{\tilde{\alpha}_{G,B}^{n+1}}{\alpha_{G,B}^{n}}\right)^{\frac{2}{3}}, \text{ for } \alpha_{G,B} > \alpha_{NC}. \tag{5-33}$$

5.2. Droplets in Bubbly Region

The convectible IFA is $A_{Lm,B}$. The source terms modeled are

S_{WD} : Weber number breakup of droplets,

S_{TD} : Turbulence breakup of droplets,

S_{CD} : Coalescence of droplets, and

S_{MD} : Mass transfer to droplets.

In addition, other mechanisms are also taken into account similar to Section 5.1.

5.2.1. Weber number breakup of droplets

Regarding droplet breakup due to hydrodynamic instability, two types of models are available and can be selected by the input data. The first and standard model is the AFDM type model. The source term is given by

$$S_{Lm,B,WB} = \max\left(0,\ \frac{A_{Lm,B,WB}^{e} - A_{Lm,B}}{\tau_{Lm,B,WB}}\right), \tag{5-34}$$

where the equilibrium area is

$$A^{e}_{Lm,B,WB} = \frac{3\alpha_{Lm,B}}{r^{e}_{Lm,B,WB}}. \tag{5-35}$$

If Weber number We is larger than the user-defined critical Weber number for droplets, We_D, the increase of convectible IFA by the hydrodynamic breakup of droplets is calculated by the models described below.

$$\mathrm{We} = \frac{2r_{Lm,B}\rho_{CL}\Delta v^2}{\left(\sqrt{\sigma_{CP}} - \sqrt{\sigma_{Lm}}\right)^2}, \tag{5-36}$$

where Δv is the velocity difference between vapor and continuous liquid,

$$\Delta v = max10 - 4, vq - vCP \text{ , and} \tag{5-37}$$

ρ_{CL} is the microscopic density of the continuous phase.

Two types of models are available for the time constant of breakup in the AFDM type model. The first and standard model is Taylor-type correlation[18] given by

$$\tau_{Lm,B} = C_{TWB}\mathrm{Bo}^{-0.25}, \tag{5-38}$$

where Bo is Bond number given by

$$\mathrm{Bo} = \frac{3}{16}C_{DD}\mathrm{We}, \tag{5-39}$$

and C_{DD} is the drag coefficient between the droplet and continuous liquid,

$$C_{DD} = \begin{cases} \dfrac{24}{Re_D}\left(1 + 0.125\mathrm{Re}_D{}^{0.72}\right) & \text{for } \mathrm{Re}_D < 1000 \\ 2.5 & \text{for } 1000 \le \mathrm{Re}_D \end{cases}, \text{and} \tag{5-40}$$

$$\mathrm{Re}_D = \frac{2\rho_{CL}\Delta v r_{Lm,B}}{\mu_{CP}}. \tag{5-41}$$

The second and optional model based on Pilch and Eldman[19] is also available as

$$\tau_{Lm,B} = \begin{cases} 6(\mathrm{We} - \mathrm{We}_D)^{-0.25} & \mathrm{We}_D < \mathrm{We} \le 18 \\ 2.45(\mathrm{We} - \mathrm{We}_D)^{0.25} & 18 < \mathrm{We} \le 45 \\ 14.1(\mathrm{We} - \mathrm{We}_D)^{0.25} & 45 < \mathrm{We} \le 351 \\ 0.766(\mathrm{We} - \mathrm{We}_D)^{0.25} & 351 < \mathrm{We} \le 2670 \\ 5.5 & 2670 < \mathrm{We} \end{cases}. \tag{5-42}$$

It is possible to consider the velocity decrease when the breakup completed. In this case, the velocity difference Δv is replaced with the modified velocity difference Δv_e in the evaluation of the equilibrium radius.

$$\Delta v_e = \max\left(10^{-4}, \frac{\Delta v}{1 + 0.75C_{DD}C_{\rho}\tau_{Lm,B,WB}}\right), \tag{5-43}$$

where C_{ρ} is given by,

$$C_\rho = \sqrt{\frac{\rho_{CL}}{\rho_{Lm}}}. \tag{5-44}$$

The equilibrium radius and time constant are obtained as

$$r^e_{Lm,B,WB} = \frac{C_{FDB}\mathrm{We}_D\left(\sqrt{\sigma_{CP}} - \sqrt{\sigma_{Lm}}\right)^2}{2\rho_{CL}\Delta v^2}\ , \text{and} \tag{5-45}$$

$$\tau_{Lm,B,WB} = \frac{2C_{FSB}r_{Lm,B}}{\Delta v C_\rho}\tau_{Lm,B}\ . \tag{5-46}$$

Another optional model for droplet breakup due to hydrodynamic instability is the IFCI type model[20]. The source term is given by

$$S_{Lm,B,WB} = -A^{\rho_{Lm,B,WB}}_{Lm,B}\Gamma_{Lm,B,WB}\ . \tag{5-47}$$

If Weber number We is larger than the user-defined critical Weber number for droplets, We_D, the increase of convectible IFA by the hydrodynamic breakup of droplets is calculated by the models described below.

$$\mathrm{We} = \frac{2r_{Lm,B}\rho_F {\Delta v_F}^2}{\left(\sqrt{\sigma_{CP}} - \sqrt{\sigma_{Lm}}\right)^2}, \tag{5-48}$$

where Δv_F is the velocity difference between vapor and continuous liquid,

$$\Delta v_F = \max\left(10^{-4}, \sqrt{\left(V_{Lm,CF} - V_{CP}\right)^2 + \left(U_{Lm,CF} - U_{CP}\right)^2}\right), \tag{5-49}$$

$$V_{LM,CF} = \frac{\alpha_{Lm}V_{Lm} + \alpha_{CP}V_{CP}}{\alpha_{Lm} + \alpha_{CP}}, \tag{5-50}$$

$$U_{LM,CF} = \frac{\alpha_{Lm}U_{Lm} + \alpha_{CP}U_{CP}}{\alpha_{Lm} + \alpha_{CP}}\ , \text{and} \tag{5-51}$$

$$\rho_F = \frac{\alpha_{Lm}\rho_{Lm} + \alpha_{CP}\rho_{CP}}{\alpha_{Lm} + \alpha_{CP}}, \tag{5-52}$$

and subscript CP corresponds to the continuous phase. The coefficient and variable in Eq. (5-47) are given by,

$$\rho_{Lm,B,WB} = 2\ , \text{and} \tag{5-53}$$

$$\Gamma_{Lm,B,WB} = \frac{-C_{CO}\Delta v_F C_\rho}{6\alpha_{Lm,B}}, \tag{5-54}$$

where the coefficient C_{CO} is obtained by,

$$C_{CO} = \begin{cases} 0.245 & \text{for IFCI type model}\,^{20)} \\ \dfrac{1}{3\tau_{AL}} & \text{for Esprose type model}\,^{21)} \end{cases}, \tag{5-55}$$

$$\tau_{AL} = 13.7\mathrm{Bo}^{-0.25}\,, \tag{5-56}$$

$$\mathrm{Bo} = \frac{3}{16} C_D \mathrm{We}\,, \tag{5-57}$$

$$C_D = \begin{cases} \dfrac{24}{\mathrm{Re}}(1 + 0.125Re^{0.72}) & \text{for Re} < 1000 \\ 2.5 & \text{for } 1000 \leq \mathrm{Re} \end{cases}, \text{and} \tag{5-58}$$

$$\mathrm{Re} = \frac{2\rho_{CP}\Delta v_F r_{Lm,B}}{\mu_{CP}}. \tag{5-59}$$

5.2.2. Turbulence breakup of droplets

The experience in AFDM suggests that droplets coexisting with bubbles in a continuous liquid cell should be fragmented with the same turbulence velocity. The source term is

$$S_{Lm,B,TB} = \max\left(0,\ \frac{A^e_{Lm,B,TB} - A_{Lm,B}}{\tau_{Lm,B,TB}}\right). \tag{5-60}$$

Based on AFDM, this criterion for the lowest eigen frequency is given by

$$r_{e,TD} = \left(\frac{24}{31}\frac{2^{\frac{2}{3}}\sigma_{CP}}{3\rho_{Lm} + 2\rho_{CP}}\frac{1}{v'v'}\right)^{\frac{1}{3}}, \tag{5-61}$$

where $v'v'$ is the square of the turbulence velocity, and the time constant is given by

$$\tau_{TD} = \frac{2r_{Lm,B}}{\sqrt{v'v'}}. \tag{5-62}$$

The same formulation as the bubble breakup is used for $v'v'$.

$$v'v' = Cr_{Lm,B}{}^2\left\{\left[\frac{\partial(u_{Lm} - u_{CP})}{\partial z}\right]^2 + \left[\frac{\partial(v_{Lm} - v_{CP})}{\partial r}\right]^2\right\}. \tag{5-63}$$

If the flow is restricted in a vertical channel, the turbulence breakup caused by buoyancy is modeled as follows

$$v'v' = C_{RDP}{}^2\frac{\alpha_{Lm}}{1-\alpha_S}\left(1 - \frac{\alpha_{Lm}}{1-\alpha_S}\right)\left(1 - \frac{\rho_{Lm}}{\rho_{CL}}\right)g\,. \tag{5-64}$$

A larger of Eqs. (5-63) and (5-64) is used.

5.2.3. Droplet coalescence

The SIMMER-II formula is used as

$$\frac{d}{dt}r_{Lm,B} = \frac{\omega_D v'}{8f_B(1-\alpha_S)}, \tag{5-65}$$

where ω_D is coalescence probability per one collision, and
v' is the mean velocity fluctuation of droplet.

The rate of IFA change can be deduced from this equation as follows

$$\frac{d}{dt}A_{Lm,B} = -\frac{3}{{r_{Lm,B}}^2}\frac{d}{dt}r_{Lm,B} = \frac{\omega_D {A_{Lm,B}}^2 v'}{24f_B(1-\alpha_S)}. \tag{5-66}$$

The velocity fluctuation v' is assumed to be equal to $\sqrt{v'v'}$ in the turbulence modeling in Section 5.2.2.

5.2.4. Mass transfer for droplets

During the heat and mass transfer calculations, the volume fraction of each component may change as a result of mass transfer or temperature change. The update equation is:

$$\frac{\tilde{A}_{Lm,B}^{n+1}}{\tilde{A}_{Lm,B}^{n}} = \left(\frac{\tilde{\alpha}_{Lm,B}^{n+1}}{\alpha_{Lm,B}^{n}}\right)^{\frac{2}{3}}. \tag{5-67}$$

For fuel and steel droplets or particles, the source terms due to the breakup of structure components also need to be modeled. Although these source terms should be based on the breakup phenomenology, a preliminary model uses user-defined constant radii $r_{Lm,BR}$. Assuming that the droplets and/or particles produced from the breakup are distributed to the bubbly and dispersed regions in proportional to the volume fraction of each region, the update equation is

$$\tilde{A}_{Lm,B}^{n+1} = \tilde{A}_{Lm,B}^{n} + \frac{3\Delta t \Gamma_{Lm,BR} f_B}{\rho_{Lm} r_{Lm,BR}}, \tag{5-68}$$

where $\Gamma_{Lm,BR}$ is the breakup mass-transfer rate.

5.3. Droplets in Dispersed Region

The convectible IFA is $A_{Lm,B}$. The source terms are:

S_{FL} : Flashing of droplets,
S_{WD} : Weber number breakup for droplets,
S_{CD} : Coalescence for droplets,
S_{MD} : Mass transfer for droplets.

In addition, other mechanisms are also taken into account similar to Section 5.1.

5.3.1. Flashing of droplet

The source term is given by

$$S_{Lm,D,FL} = \max\left(0,\ \frac{A^e_{LM,D,FL} - A_{Lm,D}}{\tau_{Lm,D,FL}}\right), \tag{5-69}$$

where the equilibrium area is

$$A^e_{LM,D,FL} = \frac{3\alpha_{Lm,D}}{r_{e,FL}}. \tag{5-70}$$

An equilibrium radius is the maximum size of droplets that escape fragmentation. It is obtained from the force balance of surface tension and pressure difference.

$$r_{e,FL} = \frac{2\sigma_{Lm}}{\max\left(10^{-8},\ P_{sat,Lm} - P_{CELL}\right)}, \tag{5-71}$$

where σ_{Lm} is the surface tension of the liquid,
$P_{sat,Lm}$ is the saturation pressure of the liquid, and
P_{CELL} is the cell pressure.

Jacob number Ja is used to assess the departure from equilibrium and hence the rate at which equilibrium is obtained as follows:

$$\mathrm{Ja} = \frac{C_{p_{Lm}}\rho_{Lm}}{\rho_G h_{lg,Lm}} \max\left(0,\ T_{Lm} - T_{sat,m}(P)\right), \tag{5-72}$$

where $C_{p_{Lm}}$ is the constant pressure specific heat capacity,
$T_{sat,m}$ is the saturation temperature of the liquid at the cell pressure, and
$h_{lg,Lm}$ is the latent heat of vaporization.
The time constant for the breakup is

$$\tau_{e,FL} = C_{FL}\frac{C_{p_{Lm}}\rho_{Lm}{r_{Lm,D}}^2}{k_{Lm}\mathrm{Ja}}, \tag{5-73}$$

where C_{FL} is the user-defined constant, and
k_{Lm} is the thermal conductivity.

5.3.2. Weber number breakup for droplet

Regarding droplet breakup due to hydrodynamic instability, two types of models are available and can be selected by user input specification. The first model is the AFDM type model, in which the source term is given by

$$S_{Lm,D,WB} = \max\left(0,\ \frac{A^e_{Lm,D,WB} - A_{Lm,D}}{\tau_{Lm,D,WB}}\right), \tag{5-74}$$

where the equilibrium area is

$$A^e_{Lm,D,WB} = \frac{3\alpha_{Lm,D}}{r^e_{Lm,D,WB}} = \frac{6\alpha_{Lm,D}\rho_G\Delta v^2}{\mathrm{We}_D\sigma_{Lm}}. \tag{5-75}$$

If Weber number, We , is larger than the user-defined critical Weber number for droplets, We_D, the increase of convectible IFA by the hydrodynamic breakup of droplets is calculated by the models described below.

$$\mathrm{We} = \frac{2r_{Lm,D}\rho_G \Delta v^2}{\sigma_{Lm}}, \tag{5-76}$$

where Δv is the velocity difference between vapor and continuous liquid,

$$\Delta v = \max\left(10^{-4}, \left|\vec{v}_q - \vec{v}_G\right|\right). \tag{5-77}$$

Two types of models are available for the time constant of breakup in the AFDM type model. The first model is Taylor-type correlation[18] given by

$$\tau_{Lm,D} = C_{TWB}\mathrm{Bo}^{-0.25}, \tag{5-78}$$

Where Bo is Bond number given by,

$$\mathrm{Bo} = \frac{3}{16}C_{DD}\mathrm{We}, \tag{5-79}$$

C_{DD} is the drag coefficient between the droplet and continuous liquid,

$$C_{DD} = \begin{cases} \dfrac{24}{\mathrm{Re}_D}\left(1 + 0.125{\mathrm{Re}_D}^{0.72}\right) & \text{for } \mathrm{Re}_D < 1000 \\ 2.5 & \text{for } 1000 \le \mathrm{Re}_D \end{cases}, \text{and} \tag{5-80}$$

$$\mathrm{Re}_D = \frac{2\rho_G \Delta v r_{Lm,D}}{\mu_G}. \tag{5-81}$$

Another formulation by Pilch and Eldman[19] is also available as

$$\tau_{Lm,D} = \begin{cases} 6(\mathrm{We} - \mathrm{We}_D)^{-0.25} & \mathrm{We}_D < \mathrm{We} \le 18 \\ 2.45(\mathrm{We} - \mathrm{We}_D)^{0.25} & 18 < \mathrm{We} \le 45 \\ 14.1(\mathrm{We} - \mathrm{We}_D)^{0.25} & 45 < \mathrm{We} \le 351 \\ 0.766(\mathrm{We} - \mathrm{We}_D)^{0.25} & 351 < \mathrm{We} \le 2670 \\ 5.5 & 2670 < \mathrm{We} \end{cases}. \tag{5-82}$$

It is possible to consider the velocity decrease when the breakup completed. In this case, the velocity difference Δv is replaced by the modified velocity difference Δv_e in the evaluation of the equilibrium radius.

$$\Delta v_e = \begin{cases} \Delta v\left[1 - \left(0.375\tau_{Lm,D,WB} + 3 \times 0.0758{\tau_{Lm,D,WB}}^2\right)C_\rho\right] & \text{for } \mathrm{Ma} \le 0.5 \\ \Delta v\left[1 - \left(0.75\tau_{Lm,D,WB} + 3 \times 0.116{\tau_{Lm,D,WB}}^2\right)C_\rho\right] & \text{for } 0.5 < \mathrm{Ma} \end{cases}, \tag{5-83}$$

where C_ρ and Mach number Ma are given by,

$$C_\rho = \sqrt{\frac{\rho_G}{\rho_{Lm}}}, \text{and} \tag{5-84}$$

$$\mathrm{Ma} = \frac{\Delta v}{v_{sound,G}}. \tag{5-85}$$

The equilibrium radius and time constant are obtained as

$$r^{e}_{Lm,D,WB} = \frac{C_{FDD}\mathrm{We}\sigma_{Lm}}{2\rho_G \Delta v^2}\ , \text{and} \tag{5-86}$$

$$\tau_{Lm,D,WB} = \frac{2C_{FSD}r_{Lm,D}}{\Delta v C_\rho}\tau_{Lm,D}\ . \tag{5-87}$$

Another model for droplet breakup due to hydrodynamic instability is the IFCI type model [20]. The source term is given by

$$S_{Lm,B,WB} = -A^{\rho_{Lm,B,WB}}_{Lm,B}\Gamma_{Lm,B,WB}\ . \tag{5-88}$$

In this model, the increase of convectible IFA by the hydrodynamic breakup of droplets is calculated, if Weber number, given by the following formula, is larger than the user-defined critical Weber number for droplets, We_D.

$$\mathrm{We} = \frac{2r_{Lm,B}\rho_F {\Delta v_F}^2}{\left(\sqrt{\sigma_{CP}} - \sqrt{\sigma_{Lm}}\right)^2}, \tag{5-89}$$

where Δv_F is the velocity difference between vapor and continuous liquid,

$$\Delta v_F = \max\left(10^{-4}, \sqrt{\left(V_{Lm,CF} - V_{CP}\right)^2 + \left(U_{Lm,CF} - U_{CP}\right)^2}\right), \text{with} \tag{5-90}$$

$$V_{LM,CF} = \frac{\alpha_{Lm}V_{Lm} + \alpha_{CP}V_{CP}}{\alpha_{Lm} + \alpha_{CP}}, \tag{5-91}$$

$$U_{LM,CF} = \frac{\alpha_{Lm}U_{Lm} + \alpha_{CP}U_{CP}}{\alpha_{Lm} + \alpha_{CP}}\ , \text{and} \tag{5-92}$$

$$\rho_F = \frac{\alpha_{Lm}\rho_{Lm} + \alpha_{CP}\rho_{CP}}{\alpha_{Lm} + \alpha_{CP}}, \tag{5-93}$$

and subscript CP corresponds to the continuous phase.

The coefficient and variable in Eq. (5-88) are given by

$$\rho_{Lm,B,WB} = 2\ , \text{and} \tag{5-94}$$

$$\Gamma_{Lm,B,WB} = \frac{-C_{CO}\Delta v_F C_\rho}{6\alpha_{Lm,B}}, \tag{5-95}$$

where the coefficient C_{CO} is obtained by,

$$C_{CO} = \begin{cases} 0.245 & \text{for IFCI type model } [20] \\ \dfrac{1}{3\tau_{AL}} & \text{for Esprose type model } [21] \end{cases}, \text{with} \tag{5-96}$$

$$\tau_{AL} = 13.7\mathrm{Bo}^{-0.25}, \tag{5-97}$$

$$\mathrm{Bo} = \frac{3}{16} C_D \mathrm{We}, \tag{5-98}$$

$$C_D = \begin{cases} \dfrac{24}{\mathrm{Re}}(1 + 0.125\mathrm{Re}^{0.72}) & \text{for } \mathrm{Re} < 1000 \\ 2.5 & \text{for } 1000 \leq \mathrm{Re} \end{cases}, \text{and} \tag{5-99}$$

$$\mathrm{Re} = \frac{2\rho_{CP}\Delta v_F r_{Lm,B}}{\mu_{CP}}. \tag{5-100}$$

5.3.3. Droplet coalescence

The SIMMER-II formula also used in SIMMER-III is

$$\frac{d}{dt} r_{Lm,D} = \frac{\omega_D v'}{8 f_D (1 - \alpha_S)}, \tag{5-101}$$

where ω_D is the coalescence probability per collision (default: 1.0), and
v' is the mean velocity fluctuation of droplet.

The rate of IFA change is deduced from this equation as follows

$$\frac{d}{dt} A_{Lm,D} = -\frac{3}{{r_{Lm,D}}^2} \frac{d}{dt} r_{Lm,D} = \frac{\omega_D {A_{Lm,D}}^2 v'}{24 f_D (1 - \alpha_S)}. \tag{5-102}$$

The velocity fluctuation, v', is difficult to obtain. Because the density ratio of the dispersed to continuous phase is large, $\sqrt{v'v'}$ of the continuous phase cannot be used as v' for droplet. For the present modeling, it is assumed that the ratio of velocity fluctuation is equal to the microscopic density ratio. Then, the velocity fluctuation is given by

$${v'}_{Lm} = \frac{\rho_G}{\rho_{Lm}} \sqrt{{v'}_G {v'}_G}, \tag{5-103}$$

where $\sqrt{{v'}_G {v'}_G}$ is the velocity fluctuation of the vapor calculated similarly to that of continuous liquid component.

5.3.4. Mass transfer for droplets

During the heat and mass transfer calculations, the volume fraction of each component may change as a result of mass transfer or temperature change. The update equation is

$$\frac{\tilde{A}_{Lm,D}^{n+1}}{\tilde{A}_{Lm,D}^{n}} = \left(\frac{\tilde{\alpha}_{Lm,D}^{n+1}}{\alpha_{Lm,D}^{n}}\right)^{\frac{2}{3}}. \tag{5-104}$$

For fuel and steel droplets or particles, the source terms due to the breakup of structure components also need to be modeled. Although these source terms should be based on the breakup phenomenology, a preliminary model uses user-defined constant radii $r_{Lm,BR}$. The update equation is

$$\tilde{A}_{Lm,D}^{n+1} = \tilde{A}_{Lm,D}^{n} + \frac{3\Delta t \Gamma_{Lm,BR} f_D}{\rho_{Lm} r_{Lm,BR}}, \tag{5-105}$$

where $\Gamma_{Lm,BR}$ is the breakup mass-transfer rate.

5.4. Source Terms Specific to Channel Flow

Currently only the droplet entrainment in the annular-dispersed flow is modeled in SIMMER-III. Other possible source terms in the slug flow and the other channel flow regimes are judged to be negligible or less important.

S_{DE} : Droplet entrainment in the annular-dispersed flow.

Although turbulence breakup caused by wall shear stress may be considered here similarly to the previous sections, this mechanism is not directly modeled in the current version of SIMMER-III.

In the annular-dispersed (flooding transition) flow regime, droplet entrainment or deposition (or de-entrainment) occurs at the boundary of the liquid continuous region and the vapor continuous region. The entrainment or deposition associates the production, loss, and/or diffusion of the convectible IFAs of droplets in each continuous region. The entrained droplets are assumed to break up instantaneously by dynamic force and hence the equilibrium radius defined by Eq. (5-75) for Weber number breakup is also used as the entrainment radius $r_{e,WB}$. The radii of deposited droplets are assumed to be equal to the values in the dispersed region. Assuming that the fractions of the entrained components are proportional to the volume fractions in the cell, the source terms are defined as follows:

$$S_{CP,B,DE} = 0 \text{ , and} \tag{5-106}$$

$$S_{Lm,D,DE} = \begin{cases} -\dfrac{dE_r}{dt}\dfrac{3\alpha_{Lm}}{r_{e,WB}} & \text{for } \dfrac{dE_r}{dt} \geq 0 \\ -\dfrac{dE_r}{dt}\dfrac{A_{Lm,D}}{f_D} & \text{for } \dfrac{dE_r}{dt} < 0 \end{cases} \quad \text{for } m \neq CP \text{ .} \tag{5-107}$$

These source terms are defined only for the real liquids (m=1, 2, 3) because the convectible IFAs of particles (m=4, 5, 7) are not treated separately in the two regions.

5.5. Interfacial Area Update

The convection equation for a convectible IFA is shown again,

$$\frac{\partial A_f}{\partial t} + \nabla \cdot \left(\vec{v}_{q(f)} A_f\right) = \sum_k S_{f,k} - A_{f,B\leftrightarrow D}\,, \tag{5-1}$$

The convectible IFAs are updated in three steps. First, Eq. (5-1) is solved with source terms but without the convection terms in fluid-dynamics Step 1. Second, after the heat and mass transfer operations, the same equation is solved with additional source terms from heat and mass transfer. This is done at the very end of Step 1. Third, the source terms are set to zero and the IFAs are convected with end-of-time-step velocities in fluid-dynamics Step 4. The IFA of bubbles is also adjusted at the same time to take into account the change of vapor microscopic densities.

Generally, the formulations of source terms in SIMMER-III are written as

$$S_k = \frac{A_{ek} - A_f}{\tau_k} \quad \text{or} \quad S_l = -A_f^{\rho_l} \Gamma_l \,. \tag{5-108}$$

In the update calculation using these source terms, an implicit algorithm is adopted to avoid overshooting of the areas in the case of large A_{ek} or small τ_k. Making an approximation that

$$A^{\rho_l} = \tilde{A}^{n+1} (A^n)^{\rho_l - 1} \,, \tag{5-109}$$

the updating formula is:

$$\tilde{A}^{n+1} = \left(A_f^n + \Delta t \sum_{A_{ek} > A_f} \frac{A_{ek}}{\tau_k} \right) \Bigg/ \left\{ 1 + \Delta t \left[\sum_{A_{ek} > A_f} \frac{1}{\tau_k} + \sum_l (A^n)^{\rho_l - 1} \Gamma_l \right] \right\} . \tag{5-110}$$

The equilibrium areas based on breakup criteria correspond to the maximum radius which can escape fragmentation and therefore the mechanism which produces the largest area becomes dominant under the equilibrium condition. Therefore, the source terms based on breakup criteria must not be averaged. Instead, the breakup source terms of which the equilibrium area is smaller than the present convectible area are excluded from the summation in Eq. (5-110) to prevent the convectible IFA from being dominated by the source terms with small A_{ek} and small τ_k.

6. Binary Contact Areas

To perform the heat and mass transfer operations and to calculate momentum exchange functions, IFAs are needed for each of the 52 possible contact modes for seven liquid energy components, vapor components, and three structure surfaces (a fuel pin, left can wall and right can wall) for SIMMER-III (68 contacts for SIMMER-IV). Such binary contact areas are defined using the convectible IFAs, structure surface areas, volume fractions, physical properties and input parameters. Figure 12 illustrates all the binary contact modes treated in the present SIMMER-III model. In this chapter, the fluid-structure contact modes are described first and the fluid-fluid contact modes second.

6.1. Fluid-structure Contacts

The present model calculates the fluid-structure contact areas based on the volume fractions of the fluids and the "summation rule" that the sum of contact areas over a component should be equal to the convectible IFA of the component,

$$A_M = \sum_{K \neq M} a_{M,K} \tag{3-4}$$

where A_M is a convectible IFA of the component *M*, and
$a_{M,K}$ is a contact area of the component *M* with the other component *K*.
Although there may exist some influences of the surface tension, fluid wetting characteristics, and other physical properties, modeling these effects is judged to be beyond the scope of the current IFA and is left for the future studies.

6.1.1. Droplet-structure contacts

The droplet-structure contact areas are assumed to be proportional to the volume fraction of the droplets. The contact areas of dispersed liquid (*m* = *DP*, 4, 5, 6, 7) and "film" structure are

$$\alpha_{Lm,FS,B} = C_{Lm,S} \frac{\alpha_{Lm,B}}{\alpha_{F,B}} \min\left(A_{Lm,B}, A_{FS,B}\right), \tag{6-1a}$$

$$a_{Lm,FS,B1} = f_{B1} a_{Lm,FS,B}, \tag{6-1b}$$

$$a_{Lm,FS,B2} = f_{B2} a_{Lm,FS,B}, \tag{6-1c}$$

$$a_{Lm,FS,D} = C_{Lm,S} \frac{\alpha_{Lm,D}}{\alpha_{F,D}} \min\left(A_{Lm,D}, A_{FS,D}\right), \text{and} \tag{6-1d}$$

$$a_{Lm,FS} = a_{Lm,FS,B} + a_{Lm,FS,D}, \tag{6-1e}$$

where $C_{Lm,S}$ is an input parameter, with the default of 0.5 is suggested based on the AFDM formulation. The contact areas of dispersed liquid (*m* = *DP*, 4, 5, 6, 7) and "vapor" structure can be obtained in the same way. These are

$$a_{Lm,VS,B} = C_{Lm,S}\frac{\alpha_{Lm,B}}{\alpha_{F,B}}\min\left(A_{Lm,B}, A_{VS,B}\right), \tag{6-2a}$$

$$a_{Lm,VS,B1} = f_{B1}a_{Lm,VS,B}, \tag{6-2b}$$

$$a_{Lm,VS,B2} = f_{B2}a_{Lm,VS,B}, \tag{6-2c}$$

$$a_{Lm,VS,D} = C_{Lm,S}\frac{\alpha_{Lm,D}}{\alpha_{F,D}}\min\left(A_{Lm,D}, A_{VS,D}\right), \text{and} \tag{6-2d}$$

$$a_{Lm,VS} = a_{Lm,VS,B} + a_{Lm,VS,D}. \tag{6-2e}$$

The droplets of component *CP* exist in the *CP*2-continuous region and the dispersed region. Their contact areas with the structure are calculated as

$$a_{CP,FS,B2} = C_{CP,S}\frac{\alpha_{CP,B2}}{f_{B2}\alpha_{F,B}}\min\left(A_{CP,B2}, A_{FS,B2}\right), \tag{6-3a}$$

$$a_{CP,FS,D} = C_{CP,S}\frac{\alpha_{CP,D}}{\alpha_{F,D}}\min\left(A_{CP,D}, A_{FS,D}\right), \tag{6-3b}$$

$$a_{CP,VS,B2} = C_{CP,S}\frac{\alpha_{CP,B2}}{f_{B2}\alpha_{F,B}}\min\left(A_{CP,B2}, A_{VS,B2}\right), \text{and} \tag{6-3c}$$

$$a_{CP,VS,D} = C_{CP,S}\frac{\alpha_{CP,D}}{\alpha_{F,D}}\min\left(A_{CP,D}, A_{VS,D}\right). \tag{6-3d}$$

The droplets of component *CP*2 exist in the *CP*-continuous region and the dispersed region. Their contact areas with the structure are also calculated as

$$a_{CP2,FS,B1} = C_{CP,S}\frac{\alpha_{CP2,B1}}{f_{B1}\alpha_{F,B}}\min\left(A_{CP2,B1}, A_{FS,B1}\right), \tag{6-4a}$$

$$a_{CP2,FS,D} = C_{CP,S}\frac{\alpha_{CP2,D}}{\alpha_{F,D}}\min\left(A_{CP2,D}, A_{FS,D}\right), \tag{6-4b}$$

$$a_{CP2,VS,B1} = C_{CP2,S}\frac{\alpha_{CP2,B1}}{f_{B1}\alpha_{F,B}}\min\left(A_{CP2,B1}, A_{VS,B1}\right), \text{and} \tag{6-4c}$$

$$a_{CP2,VS,D} = C_{CP2,S}\frac{\alpha_{CP2,D}}{\alpha_{F,D}}\min\left(A_{CP2,D}, A_{VS,D}\right). \tag{6-4d}$$

6.1.2. Vapor-structure contacts

The vapor-structure contact mode in the bubbly region is the same as the droplet-structure contact and hence the similar expression can be adopted. For the contact with the “film” structure,

$$a_{G,FS,B} = C_{G,S}\frac{\alpha_{G,B}}{\alpha_{F,B}}\min\left(A_{G,B}, A_{FS}\right), \tag{6-5a}$$

$$a_{G,FS,B1} = f_{B1}\alpha_{G.FS,B}\text{, and} \tag{6-5b}$$

$$a_{G,FS,B2} = f_{B2}\alpha_{G.FS,B}, \tag{6-5c}$$

where $C_{G,S}$ is input parameters, with the default of 0.5.

On the other hand, the vapor-structure contact area in the dispersed region is obtained from the volume fraction consideration and the limiting value which stems from the summation rule.

$$a_{G,FS,D} = \max\left(C_{G,S}\frac{\alpha_{G,D}}{\alpha_{F,D}}A_{FS,D}, A_{FS,D} - \sum_{m=1}^{7} a_{Lm,FS,D}\right). \tag{6-6}$$

The total vapor-"film structure" contact area becomes

$$a_{G,FS} = \alpha_{G.FS,B} + \alpha_{G.FS,D}. \tag{6-7}$$

The contact area of vapor and "vapor structure" is obtained similarly. These are

$$a_{G,VS,B} = C_{G,S}\frac{\alpha_{G,B}}{\alpha_{F,B}}\min\left(A_{G,B}, A_{VS,B}\right), \tag{6-8a}$$

$$a_{G,VS,B1} = f_{B1}\alpha_{G.VS,B}, \tag{6-8b}$$

$$a_{G,VS,B2} = f_{B2}\alpha_{G.VS,B}, \tag{6-8c}$$

$$a_{G,VS,D} = \max\left(C_{G,S}\frac{\alpha_{G,D}}{\alpha_{F,D}}A_{VS,D}, A_{VS,D} - \sum_{m=1}^{7} a_{Lm,VS,D}\right)\text{, and} \tag{6-8d}$$

$$a_{G,VS} = \alpha_{G.VS,B} + \alpha_{G.VS,D}. \tag{6-8e}$$

6.1.3. Continuous liquid-structure contacts

The contact areas between the continuous liquids (*m*=*CP*, *CP*2) and the structure in the bubbly region are defined in the same manner as the vapor-structure contact area in the dispersed region. Namely,

$$a_{CP,FS,B1} = \max\left(C_{CP,S}\frac{\alpha_{CP,B1}}{f_{B1}\alpha_{F,B}}A_{FS,B1}, A_{FS,B1} - \sum_{L=1}^{7} a_{Lm,FS,B1} - a_{G,FS,B1}\right), \tag{6-9a}$$

$$a_{CP,FS,B} = a_{CP,FS,B1} + a_{CP,FS,B2}, \tag{6-9b}$$

$$a_{CP,FS} = a_{CP,FS,B} + a_{CP,FS,D}, \tag{6-9c}$$

$$a_{CP,VS,B1} = \max\left(C_{CP,S}\frac{\alpha_{CP,B1}}{f_{B1}\alpha_{F,B}}A_{VS,B1}, A_{VS,B1} - \sum_{\substack{m=1 \\ m\neq CP}}^{7} a_{Lm,VS,B1} - a_{G,VS,B1} \right), \tag{6-10a}$$

$$a_{CP,VS,B} = a_{CP,VS,B1} + a_{CP,VS,B2}\,, \tag{6-10b}$$

$$a_{CP,VS} = a_{CP,VS,B} + a_{CP,VS,D}\,, \tag{6-10c}$$

$$a_{CP2,FS,B2} = \max\left(C_{CP2,S}\frac{\alpha_{CP2,B2}}{f_{B2}\alpha_{F,B}}A_{FS,B2}, A_{FS,B2} - \sum_{\substack{m=1 \\ m\neq CP2}}^{7} a_{Lm,FS,B2} - a_{G,FS,B2} \right), \tag{6-11a}$$

$$a_{CP2,FS,B} = a_{CP2,FS,B1} + a_{CP2,FS,B2}\,, \tag{6-11b}$$

$$a_{CP2,FS} = a_{CP2,FS,B} + a_{CP2,FS,D}\,, \tag{6-11c}$$

$$a_{CP2,VS,B2} = \max\left(C_{CP2,S}\frac{\alpha_{CP2,B2}}{f_{B2}\alpha_{F,B}}A_{VS,B2}, A_{VS,B2} - \sum_{\substack{m=1 \\ m\neq CP2}}^{7} a_{Lm,VS,B2} - a_{G,VS,B2} \right), \tag{6-12a}$$

$$a_{CP2,VS,B} = a_{CP2,VS,B1} + a_{CP2,VS,B2}\,, \text{and} \tag{6-12b}$$

$$a_{CP2,VS} = a_{CP2,VS,B} + a_{CP2,VS,D}\,. \tag{6-12c}$$

6.1.4. Assignment to structure components

The fluid-structure contact areas are partitioned to the structure energy components based on the fractions of their surface areas and parameter *ILS* (See Section 3.1.2). For example, the liquid-PIN structure contact area in SIMMER-III is obtained from

$$a_{Lm,PIN} = \begin{cases} a_{Lm,FS} & : ILS = 1 \\ a_{Lm,VS}\dfrac{A_{PIN}}{A_{PIN}+A_{RC}} & : ILS = 2 \\ a_{Lm,VS}\dfrac{A_{PIN}}{A_{PIN}+A_{LC}} & : ILS = 3 \\ a_{Lm,FS}\dfrac{A_{PIN}}{A_{PIN}+A_{LC}} & : ILS = 4\,. \\ a_{Lm,FS}\dfrac{A_{PIN}}{A_{PIN}+A_{RC}} & : ILS = 5 \\ a_{Lm,VS} & : ILS = 6 \\ a_{Lm,FS}\dfrac{A_{PIN}}{A_{PIN}+A_{LC}+A_{RC}} & : ILS = 7 \end{cases} \tag{6-13a}$$

Similar expressions can be derived for $a_{Lm,LC}$, $a_{Lm,RC}$, $a_{G,PIN}$, $a_{G,LC}$, and $a_{G,RC}$.

The same procedure is applied to the partitioning of structure surface in SIMMER-IV based on the fractions of their surface areas and parameter *ILS* (See Section 3.1.2). For example, the liquid-PIN structure contact area in SIMMER-IV is obtained from

$$a_{Lm,PIN} = \begin{cases} a_{Lm,FS} & : ILS = 1 \\ a_{Lm,VS} & : ILS = 2 \\ a_{Lm,VS}\dfrac{A_{PIN}}{A_{PIN} + A_{LC} + A_{RC} + A_{FC} + A_{BC}} & : ILS = 3 \end{cases}. \tag{6-13b}$$

Similar expressions can be derived for $a_{Lm,LC}$, $a_{Lm,RC}$, $a_{Lm,FC}$, and $a_{Lm,BC}$.

6.2. Fluid-fluid Contacts

The models to calculate fluid-fluid contact areas are commonly used in SIMMER-III and SIMMER-IV. Five contact modes are considered for fluid-fluid contacts: the dispersed/dispersed fluids, the droplets/vapor, the droplets/continuous liquid, the bubbles/continuous liquid, and the continuous liquid/vapor contacts. For the fluid-fluid contacts between moving discontinuous components, a theory used in SIMMER-II[3] is used. For the contacts involving continuous components, the contact areas are obtained from the volume fraction consideration and the limiting value which stems from the "summation rule". The effects of other physical properties such as surface tension may exist, but inclusion of these effects is decided to be left for future efforts.

The basic contact formula adopted for spheres of discontinuous components moving at a different or same velocity and touching for a collision time is

$$\hat{a}_{M,K,R} = \frac{6}{19}\frac{\alpha_{M,R}\alpha_{K,R}}{\alpha_{F,R}}\frac{r_{M,R} + r_{K,R}}{r_{M,R}r_{K,R}\max\left({r_{M,R}}^2, {r_{K,R}}^2\right)}{\hat{r}_{M,K,R}}^2, \tag{6-14}$$

where

$${\hat{r}_{M,K,R}}^2 = \frac{{r_{M,R}}^2|\vec{v}_M| + {r_{K,R}}^2|\vec{v}_K|}{\max\left(|\vec{v}_K - \vec{v}_M|,\ \frac{1}{4}|\vec{v}_K + \vec{v}_M|\right)}, \text{ and} \tag{6-15}$$

subscripts *M* and *K* denote the energy components *M* and *K*, respectively, subscript *F* denotes the flow area, and subscript *R* denotes the flow area to which this formula is applied.

Other formulas might be possible, particularly if the effects of velocity fluctuations are to be explicitly accommodated by some turbulence modeling.

6.2.1. Contacts between dispersed fluids

The contact areas of dispersed phases (*m* = *DP*, 4, 5, 6, 7) with other dispersed fluids are based on the contact formula and the limiting value determined from the volume fractions. These are described below.

For droplet-droplet contacts, for *m*=*DP*, 4, 5, 6, 7,

$$a_{Lm,Lk,B} = C_{Lm,Lk}\min\left(A_{Lk,B}\frac{\alpha_{Lm}}{\alpha_{F,B}}, A_{Lm,B}\frac{\alpha_{Lk}}{\alpha_{F,B}},\ \hat{a}_{Lm,Lk,B}\right), \tag{6-16a}$$

$$a_{Lm,Lk,D} = C_{Lm,Lk}\min\left(A_{Lk,D}\frac{\alpha_{Lm}}{\alpha_{F,D}}, A_{Lm,D}\frac{\alpha_{Lk}}{\alpha_{F,D}},\ \hat{a}_{Lm,Lk,D}\right), \tag{6-16b}$$

$$a_{Lm,Lk,B1} = f_{B1}a_{Lm,Lk,B}\ , \tag{6-16c}$$

$$a_{Lm,Lk,B2} = f_{B2}a_{Lm,Lk,B}\ , \tag{6-16d}$$

$$a_{Lm,CP,B2} = C_{Lm,CP}\min\left(A_{CP,B2}\frac{\alpha_{Lm}}{\alpha_{F,B}}, A_{Lm,B2}\frac{\alpha_{CP,B2}}{f_{B2}\alpha_{F,B}},\ \hat{a}_{Lm,CP,B2}\right), \text{and} \tag{6-16e}$$

$$a_{Lm,CP2,B1} = C_{Lm,CP2}\min\left(A_{CP2,B1}\frac{\alpha_{Lm}}{\alpha_{F,B}}, A_{Lm,B1}\frac{\alpha_{CP2,B1}}{f_{B1}\alpha_{F,B}},\ \hat{a}_{Lm,CP2,B1}\right). \tag{6-16f}$$

For droplet-bubble contacts,

$$a_{Lm,G,B} = C_{Lm,G}\min\left(A_{G,B}\frac{\alpha_{Lm,B}}{\alpha_{F,B}}, A_{Lm,B}\frac{\alpha_{G,B}}{\alpha_{F,B}},\ \hat{a}_{Lm,G,B}\right), \tag{6-17a}$$

$$a_{Lm,G,B1} = f_{B1}a_{Lm,G,B}\ , \tag{6-17b}$$

$$a_{Lm,G,B2} = f_{B2}a_{Lm,G,B}\ , \tag{6-17c}$$

$$a_{CP,G,B2} = C_{CP,G}\min\left(A_{G,B2}\frac{\alpha_{CP,B2}}{f_{B2}\alpha_{F,B}}, A_{CP,B2}\frac{\alpha_{G,B}}{\alpha_{F,B}},\ \hat{a}_{CP,G,B2}\right), \text{and} \tag{6-17d}$$

$$a_{CP2,G,B1} = C_{CP2,G}\min\left(A_{G,B1}\frac{\alpha_{CP2,B1}}{f_{B1}\alpha_{F,B}}, A_{CP2,B1}\frac{\alpha_{G,B}}{\alpha_{F,B}},\ \hat{a}_{CP2,G,B1}\right), \tag{6-17e}$$

6.2.2. Contacts between droplets and continuous vapor

There are two elements for a contact area between droplets and vapor. One is the contact area in the dispersed region and the other is the contact area through the interface of the bubbly and dispersed region. The former contact area is obtained by the summation argument with a limiter.

$$a_{Lm,G,D} = \max\left(C_{Lm,G}\frac{\alpha_{G,D}}{\alpha_{F,D}}A_{Lm,G}, A_{Lm,D} - a_{Lm,FS,D} - a_{Lm,VS,D} - \sum_{\substack{k=1\\k\neq m}}^{7} a_{Lm,Lk,D}\right), \tag{6-18}$$

for m = 1 ~ 7. The droplet-vapor contact areas from the latter mode are obtained from the volume fraction consideration, for *m*=*DP*, 4, 5, 6, 7,

$$a_{Lm,G,I} = C_{Lm,G}\frac{\alpha_{Lm,B}}{\alpha_{F,B}}\min\left(A_{B,D}, A_{CP,B}\right), \tag{6-19a}$$

$$a_{Lm,G,I,B1} = f_{B1}a_{Lm,G,I}\ , \text{and} \tag{6-19b}$$

$$a_{Lm,G,I,B2} = f_{B2} a_{Lm,G,I} \,. \tag{6-19c}$$

The contact of *CP* droplets in *CP*2-continuous region and the contact of *CP*2 droplets in *CP*-continuous region are obtained from:

$$a_{CP,G,I,B2} = C_{CP,G} \frac{\alpha_{CP,B2}}{f_{B2}\alpha_{F,B}} \min\left(f_{B2} A_{B,D}, A_{CP,B2}\right), \text{and} \tag{6-20a}$$

$$a_{CP2,G,I,B1} = C_{CP,G} \frac{\alpha_{CP2,B1}}{f_{B1}\alpha_{F,B}} \min\left(f_{B1} A_{B,D}, A_{CP2,B1}\right). \tag{6-20b}$$

6.2.3. Contacts between droplets and continuous liquid

The contacts between droplets and continuous liquid mainly follow using the summation rules. Areas from the *CP*-continuous region and the *CP*2-continuous region are summed to obtain the total area in the bubbly region. These are defined, for *m* =*DP*, 4, 5, 6, 7, by

$$\begin{aligned} a_{Lm,CP,B1} = \max\Bigg(& C_{Lm,CP} \frac{\alpha_{CP,B1}}{\alpha_{F,D}} A_{Lm,B}, A_{Lm,B1} - a_{Lm,FS,B1} - a_{Lm,VS,B1} - a_{Lm,G,I,B1} \\ & - a_{Lm,G,B1} - \sum_{\substack{Lk=1 \\ Lk \neq Lm,CP}}^{7} a_{Lm,Lk,B1} \Bigg), \end{aligned} \tag{6-21a}$$

$$a_{Lm,CP,B} = a_{Lm,CP,B1} + a_{Lm,CP,B2}\,, \tag{6-21b}$$

$$\begin{aligned} a_{Lm,CP2,B2} = \max\Bigg(& C_{Lm,CP2} \frac{\alpha_{CP2,B2}}{\alpha_{F,D}} A_{Lm,B}, A_{Lm,B2} - a_{Lm,FS,B2} - a_{Lm,VS,B2} - a_{Lm,G,I,B2} \\ & - a_{Lm,G,B2} - \sum_{\substack{Lk=1 \\ Lk \neq Lm,CP2}}^{7} a_{Lm,Lk,B2} \Bigg), \text{and} \end{aligned} \tag{6-21c}$$

$$a_{Lm,CP2,B} = a_{Lm,CP2,B1} + a_{Lm,CP2,B2} \,. \tag{6-21d}$$

The contact area between component *CP* and *CP*2 is obtained similarly. The expressions are:

$$\begin{aligned} a_{CP2,CP,B1} = \max\Bigg(& C_{CP2,CP} \frac{\alpha_{CP,B1}}{f_{B1}\alpha_{F,D}} A_{CP2,B1}, A_{CP2,B1} - a_{CP2,FS,B1} \\ & - a_{CP2,VS,B1} - a_{CP2,G,I,B1} - a_{CP2,G,B1} - \sum_{\substack{Lk=1 \\ Lk \neq CP,CP2}}^{7} a_{CP2,Lk,B1} \Bigg), \end{aligned} \tag{6-22a}$$

$$a_{CP,CP2,B2} = \max\left(C_{CP,CP2}\frac{\alpha_{CP2,B2}}{f_{B2}\alpha_{F,D}}A_{CP,B2}, A_{CP,B2} - a_{CP,FS,B2} - a_{CP,,VS,B2} - a_{CP,G,I,B2} - a_{CP,G,B2} - \sum_{\substack{Lk=1 \\ Lk\neq CP,CP2}}^{7} a_{CP,Lk,B2} \right), \text{and} \tag{6-22b}$$

$$a_{CP,CP2,B} = a_{CP,CP2,B1} + a_{CP,CP2,B2}\,. \tag{6-22c}$$

6.2.4. Contacts between bubble and continuous liquid

The contacts of bubbles in the *CP*-continuous region and the *CP*2-continuous region follow using a summation formula limited by the contact that should exists with the continuous phase based on the continuous phase volume fraction. The areas from *CP*-continuous region and *CP*2-continuous region are summed to obtain the areas in the bubbly region. The formulae are:

$$a_{CP,G,B1} = \max\left(C_{CP.G}\frac{\alpha_{CP,B1}}{\alpha_{F,D}}A_{G,B}, A_{G,B1} - a_{G,FS,B1} - a_{G,VS,B1} - \sum_{\substack{Lm=1 \\ Lm\neq CP}}^{7} a_{Lm,G,B1} \right), \tag{6-23a}$$

$$a_{CP,G,B} = a_{CP,G,B1} + a_{CP,G,B2}\,, \tag{6-23b}$$

$$a_{CP2,G,B2} = \max\left(C_{CP2,G}\frac{\alpha_{CP2,B2}}{\alpha_{F,D}}A_{G,B}, A_{G,B2} - a_{G,FS,B2} - a_{G,VS,B2} - \sum_{\substack{Lm=1 \\ Lm\neq CP2}}^{7} a_{Lm,G,B2} \right), \text{and} \tag{6-23c}$$

$$a_{CP2,G,B} = a_{CP2,G,B1} + a_{CP2,G,B2}\,. \tag{6-23d}$$

6.2.5. Contacts between continuous liquid and vapor

The contacts of continuous liquids with the vapor through the interface of the bubbly region and the dispersed region follow the summation formula limited by the contacts that exist with the interface based on the continuous phase volume fraction. The areas from *CP*-continuous region and *CP*2-continuous region are summed to obtain the areas in the bubbly region. The formulae are

$$a_{CP,G,I,B1} = \max\left[C_{CP.G}\frac{\alpha_{CP,B1}}{\alpha_{F,B}}A_{B,D}, f_{B1}\left(A_{B,D} - \sum_{\substack{Lm=1 \\ Lm\neq CP,CP2}}^{7} a_{Lm,G,I} \right) - a_{CP2,G,I,B1} \right], \tag{6-24a}$$

$$a_{CP,G,I} = a_{CP,G,I,B1} + a_{CP,G,I,B2}\,, \tag{6-24b}$$

$$a_{CP2,G,I,B2} = \max\left[C_{CP2.G}\frac{\alpha_{CP2,B2}}{\alpha_{F,B}}A_{B,D}, f_{B2}\left(A_{B,D} - \sum_{\substack{Lm=1 \\ Lm\neq CP,CP2}}^{7} a_{Lm,G,I}\right) - a_{CP,G,I,B1}\right], \text{and} \tag{6-24c}$$

$$a_{CP2,G,I} = a_{CP2,G,I,B1} + a_{CP2,G,I,B2}\,. \tag{6-24d}$$

7. Verification and Validation

7.1. SIMMER-III Assessment Program

A V&V program for SIMMER-III has been discussed since the beginning of the code development program. Furthermore so-called “developmental assessment” has been conducted as new models were proposed and developed. A good example is the IFA model development, where a simple test code was first developed and extensively tested for single-cell (zero-th dimension) problems before the models were actually programmed in SIMMER-III. The fluid convection algorithm and boundary conditions were also tested thoroughly in an early adiabatic version of the code without models for heat and mass transfer.

The SIMMER-III V&V program, called the “code assessment program”, was conducted in two steps, Phase 1 and Phase 2.[22), 23)] The Phase 1 assessment is intended to verify individual fluid-dynamics models of the code, whilst Phase 2 is for comprehensive validation for integral and inter-related accident phenomena, such as transient fuel motion during the transition phase and high-pressure CDA bubble expansion in the post-disassembly expansion phase. Direct application of the code to complex accident phenomena involves many inter-related processes to be solved simultaneously and is not always productive. Thus, the present stepwise approach is advantageous, since in Phase 1 the coding is largely debugged and verified, and each major model is validated separately.

7.2. Results of Phase 1 Assessment

In Phase 1 assessment[22)], SIMMER-III is applied to a variety of fluid-dynamics test problems with the objective that the individual models are validated separately as far as possible. The test problems therefore are categorized as: fluid convection algorithm, interfacial areas and momentum exchange functions, heat transfer coefficients, melting and freezing, and vaporization and condensation. In the Phase 1 report, the results of assessment on the IFA modeling were summarized as follows.

The multi-phase flow topologies are modeled by a generalized IFA convection concept, which provides a means to better simulate transient multi-phase flows because the flow history can be modeled more mechanistically rather than determining properties from instantaneous local flow conditions alone. The IFA convection model includes source terms due to liquid flashing, turbulence breakup, hydrodynamic breakup (or fragmentation), bubble nucleation and droplet/bubble coalescence. Each source term is generally characterized by an equilibrium value (for steady-state) and a time constant (for transients). These have to be estimated from experimental data.

Most of the Phase 1 assessment Problems have examined steady-state IFAs. IFAs in pool flow are discussed more fully above, with respect to the bubble column. The conclusions are that steady-state IFAs in bubbly flow are satisfactory, but bubble break-up in transition flow is rather excessive.

The two-phase blowdown problems investigated IFA source terms under highly transient conditions. SIMMER-III calculations of Edward’s pipe blowdown problem gave good agreement with experimental results without modification, but it is considered that the result is very sensitive to input parameters. It was also shown that SIMMER-III also calculates good agreement using a more physically-based bubble

nucleation model. However, it is considered that the general applicability of this nucleation model is insufficient to warrant its implementation in SIMMER-III.

In general, the overall framework of IFA modeling in SIMMER-III seems sound, though the assessment has specifically identified the need to refine the model for bubble break-up in the pool transition flow regime. The two-phase blowdown problems partly validated the IFA source term modeling, although further validation of source terms is clearly desirable. Fragmentation in FCIs is a phenomenon which is sensitive to the steady-state and transient IFA modeling. Not all the test problems studied in Phase 1 were satisfactory; many problem areas were identified and the areas of model improvement were recommended.

7.3. Results of Phase 2 Assessment

In Phase 2 assessment[23], SIMMER-III is applied to test problems relevant to key accident phenomena in LMFR such as: boiling pool dynamics, fuel relocation and freezing, material expansion, fuel-coolant interactions, structure disintegration and disrupted core neutronics. In the synthesis compiled in the Phase 2 report, the results on the assessment of the flow regime and momentum exchange models are evaluated and summarized as follow.

The multiple flow regime treatment in SIMMER-III is based on simple flow regime maps for describing both the pool and channel flows as a function of vapor volume fraction. This simple treatment can still represent a multi-component system reasonably. The Phase 1 and Phase 2 assessment programs have demonstrated that the flow regime model is mostly appropriate for describing various multi-flow topology over an entire void fraction range with smooth transition between flow regimes. The model improvement for the bubbly flow regime after Phase 1 was implemented to take into account cap-shape bubbles.

The model for IFA convection is obviously a significant technological advancement from the previous SIMMER-II. It allows us to trace the history of flow topology that changes with time and fluid flow, and thereby to simulate the transient multi-phase flows. The model together with component volume fractions provides basic information to determine the flow regime and binary contact areas between energy components. It was evaluated that the IFA convection was successfully implemented in SIMMER-III and that the application to a variety of complex multi-phase test problems was well feasible. It was recommended that the models for IFA source terms be further validated, since the modeling of IFA convection with source terms is on-going developing area and further advancement in simulation technique and experimental measurement will be available in the future.

Even with a multi-component, multi-velocity-field framework of SIMMER-III, there is a fundamental difficulty in representing an annular-dispersed flow, because a liquid component cannot be distinguished between droplets and liquid film, which have the same temperature and velocity. Needs for tracing global fluid surfaces have been desired in several areas. These include: jet or melt pour breakup in the pre-mixing phase of FCIs; entrainment of liquid droplets into a large bubble; and the splashing of a liquid surface. Modeling a global fluid surface of a length scale larger than a mesh cell size has inherent difficulty in SIMMER-III where exchange processes are described only in Step 1 (intra-cell transfer) of fluid dynamics. When such an effort is actually initiated, a modeling approach has to be carefully designed and the priority and cost-effectiveness also have to be carefully considered.

8. Conclusion

The multi-component, multi-phase flow topology and interfacial area model has been developed for the SIMMER-III and SIMMER-IV computer codes, which have been extensively utilized in LMFR CDA analyses. To systematically simulate complex flow topology, flow regime maps are modeled for both the pool flow and channel flow regimes. For the pool flow, the bubbly flow regime, the dispersed flow regime, and the transition regime containing both bubbly and dispersed regions are defined based on component volume fractions. For the channel flow, four additional flow regimes, i.e., the slug flow, the annular flow, the annular-dispersed flow, and the interpolated flow, are defined based on the volume fractions of components and the liquid entrainment fraction. With modeling the transition regime and interpolated flow regime, any transition between flow regimes is treated continuously and smoothly without abrupt change in flow properties. In a multi-component system of SIMMER-III and SIMMER-IV, all the possible contacts between components are taken into account, and the fluid-to-fluid and fluid-to-structure binary contact areas are determined for the calculations of heat and mass transfer processes and momentum-exchange functions.

Based on the preceding AFDM study, the interfacial area convection model was formulated, to enhance the flexibility of SIMMER-III by tracing the transport and history of interfaces, and thereby better representing transient physical phenomena. The changes of interfacial areas resulting from breakup, coalescence, and production of droplets or bubbles were treated as source terms of the interfacial area convection equations. This is a significant advancement in multi-phase flow simulation technology over the previous LMFR safety analysis codes such as SIMMER-II, in which interfacial areas are calculated only based on local instantaneous conditions.

Through the SIMMER-III assessment program, the code V&V effort, the interfacial area model was extensively tested against a number of basic two-phase flow problems and complex and transient multi-phase flow problems. It must be noted that the limitations of the present model have also been identified. Overall, it has been demonstrated that the interfacial area modeling was successfully implemented in SIMMER-III and SIMMER-IV and that the application to a variety of complex multi-phase problems and reactor cases is well feasible.

Acknowledgment

The authors are indebted to William R. Bohl of Los Alamos national Laboratory for formulating an overall concept and framework of SIMMER-III and for proving useful advice. They would like to acknowledge the pioneering effort by Dirk Wilhelm in his interfacial area modeling for AFDM, which formed a basis of this study. Valuable discussions with Erhard Fischer and David J. Brear, formerly working with the authors as International Fellows of PNC, were indispensable for elaborating the physical model.

The authors also would like to thank the staff of the Oarai Research and Development Institute of JAEA (the former PNC or JNC), including N. Shirakawa, K. Kamiyama, H. Yamano and T. Suzuki, for their direct or indirect contributions to this study. Special thanks go to Takamitsu Miura and Masaaki Sugaya for their tireless efforts of initial programming and extensive testing of the code.

References

1) S. Kondo, et al.: “SIMMER-III and SIMMER-IV: Computer Codes for LMFR Core Disruptive Accident Analysis,” JAEA-Research 2024-008 (2024) 235p.

2) K. Morita, et al.: “SIMMER-III Analytic Equation-of-State Model,” JNC TN9400 2000-005 (1999) 57p.

3) K. Morita, et al.: “SIMMER-III Analytic Thermophysical Property Model,” JNC TN9400 2000-004 (1999) 35p.

4) K. Morita, et al.: “SIMMER–III/IV Heat- and Mass-Transfer Model - Model and Method Description -,” JNC TN9400 2003-047 (2003) 116p.

5) K. Kamiyama, et al.: “SIMMER-III Structure Model - Model and Method Description -,” JNC TN9400 2004-043 (2004) 94p.

6) D. J. Brear, et al.: “Hear-Transfer Coefficients Model for SIMMER-III and SIMMER-IV,” JAEA-Research 2024-009 (2024) 134p.

7) Y. Tobita, et al.: “Momentum Exchange Functions Model for SIMMER-III and SIMMER-IV, ” JAEA-Research 2024-011 (2024) 39p.

8) W. R. Bohl and L. B. Luck: “SIMMER-II: “A Computer Program for LMFBR Disrupted Core Analysis,” LA-11415-MS, Los Alamos National Laboratory (1990).

9) W. R. Bohl, et al.: “AFDM: An Advanced Fluid Dynamics Model” LA-11692-MS, Los Alamos National Laboratory (1990).

10) D. Wilhelm, et al.: “AFDM: An Advanced Fluid Dynamics Model, Volume II: Topologies, Flow Regimes and Interfacial Areas” LA-11692-MS, Vol. II, Los Alamos National Laboratory (1990).

11) Y. Tobita, et al.: “Interfacial Area Modeling for a Multiphase, Multicomponent Fluid Dynamics Code,” Int. Conf. on Multiphase Flows, '91-Tsukuba, Tsukuba, Japan, Sept. 24-27 (1991).

12) W. R. Bohl, et al.: “AFDM: An Advanced Fluid Dynamics Model, Volume V: The Convective Transport Algorithm,” LA-11692-MS, Vol. V, Los Alamos National Laboratory (1990).

13) M. Ishii: “Thermo-Fluid Dynamics Theory of Two-Phase Flow,” Eyrolles, Paris (1975).

14) G. B. Wallis: “One-dimensional Two-phase Flow,” McGraw Hill, New York (1969).

15) M. Ishii and K. Mishima: “Liquid Transfer and Entrainment Correlation for Droplet-Annular Flow,” Proc. of 7th Int. Heat Trans. Conf., Munich, Germany, CONF-820901-7 (1982).

16) I. Kataoka, M. Ishii and A. Nakayama: “Entrainment and deposition rates of droplets in annular two-phase flow,” Int. J. Heat and Mass Transfer, Vol. 43, No. 9 (2000).

17) J. R. Riznic and M. Ishii: “Bubble number density and vapor generation in flashing flow,” Int. J. Heat and Mass Transfer, Vol. 32, No.10, pp.1821-1933 (1989).

18) W. W. Yuen, X. Chen and T. G. Theofanous: “On the fundamental microinteractions that support the propagation of steam explosions,” Nucl. Eng. and Des., Vol. 146, pp.133-146 (1994).

19) M. Pilch and C.A. Erdman, “Use of breakup time data and velocity history data to predict the maximum size of stable fragments for acceleration-induced breakup of a liquid drop,” Int. J. Multiphase Flow, Vol. 13, No.6, pp.741-757 (1987).

20) M. F. Young, “IFCI: An Integrated code for calculation of all phases of Fuel-Coolant Interactions,” NUREG/CR-5084; SAND-87-1048 (1987).

21) W. W. Yuen and T.G. Theofanous: “The prediction of 2D thermal detonations and resulting damage potential,” Nucl. Eng. and Des., Volume 155, pp.289-309 (1995).

22) S. Kondo, et al.: “Phase 1 Code Assessment of SIMMER-III, A Computer Program for LMFR Core Disruptive Accident Analysis,” JAEA-Research 2019-009 (2019) 382p.

23) S. Kondo, et al.: “Phase 2 Code Assessment of SIMMER-III, A Computer Program for LMFR Core Disruptive Accident Analysis,” JNC TN9400 2000-105 (2000) 777p.

Table 1. SIMMER-III/SIMMER-IV fluid-dynamics structure-field components.

Density components (MCSR)		Energy components (MCSRE)	
S-III/S-IV*		**S-III/S-IV***	
*s*1	Fertile pin fuel surface node	*S*1	Pin fuel surface node
*s*2	Fissile pin fuel surface node		
*s*3	Left fertile crust fuel	*S*2	Left crust fuel
*s*4	Left fissile crust fuel		
*s*5	Right fertile crust fuel	*S*3	Right crust fuel
*s*6	Right fissile crust fuel		
--/*s*7	Front fertile crust fuel*	--/*S*4	Front crust fuel*
--/*s*8	Front fissile crust fuel*		
--/*s*9	Back fertile crust fuel*	--/*S*5	Back crust fuel*
--/*s*10	Back fissile crust fuel*		
*S*7/s11	Cladding	*S*4/*S*6	Cladding
*S*8/*s*12	Left can wall surface node	*S*5/*S*7	Left can wall Surface node
*S*9/*s*13	Left can wall interior node	*S*6/*S*8	Left can wall Interior node
*s*10/*s*14	Right can wall surface node	*S*7/*S*9	Right can wall Surface node
*s*11/*s*15	Right can wall interior node	*S*8/*S*10	Right can wall Interior node
--/*s*16	Front can wall surface node*	--/*S*11	Front can wall surface node*
--/*s*17	Front can wall interior node*	--/*S*12	Front can wall interior node*
--/*s*18	Back can wall surface node*	--/*S*13	Back can wall surface node*
--/*s*19	Back can wall interior node*	--/*S*14	Back can wall interior node*
*s*12/*s*20	Control	*S*9/*S*15	Control

Table 2. SIMMER-III/SIMMER-IV fluid-dynamics liquid-field components.

Density components "*m*" (MCLR)		Energy components "*M*" (MCLRE)		Velocity fields "*q*" default	Velocity fields "*q*" recommended
*l*1	Liquid fertile fuel	*L*1	Liquid fuel	*q*1	*q*1
*l*2	Liquid fissile fuel			*q*1	*q*1
*l*3	Liquid steel	*L*2	Liquid steel	*q*2	*q*2
*l*4	Liquid sodium	*L*3	Liquid sodium	*q*2	*q*3
*l*5	Fertile fuel particles	*L*4	Fuel particles	*q*1	*q*1
*l*6	Fissile fuel particles			*q*1	*q*1
*l*7	Steel particles	*L*5	Steel particles	*q*1	*q*2
*l*8	Control particles	*L*6	Control particles	*q*2	*q*4
*l*9	Fertile fuel chunks	*L*7	Fuel chunks	*q*2	*q*5
*l*10	Fissile fuel chunks			*q*2	*q*5
*l*11	Fission gas in liquid fuel			*q*1	*q*1
*l*12	Fission gas in fuel particles			*q*1	*q*1
*l*13	Fission gas in fuel chunks			*q*2	*q*5

Table 3. SIMMER-III/SIMMER-IV fluid-dynamics vapor-field components.

(MCGR)		(material component) *		Velocity fields "*q*" default	Velocity fields "*q*" recommended
*g*1	Fertile fuel vapor	*G1*	Fuel vapor	*q*3	*q*6
*g*2	Fissile fuel vapor			*q*3	*q*6
*g*3	Steel vapor	*G*2	Steel vapor	*q*3	*q*6
*g*4	Sodium vapor	*G*3	Sodium vapor	*q*3	*q*6
*g*5	Fission gas	*G*4	Fission gas	*q*3	*q*6

* *All vapor components, behaving as a vapor mixture and having the same temperature, are treated as a single energy component* "*G*" *and assigned to the same velocity field.*

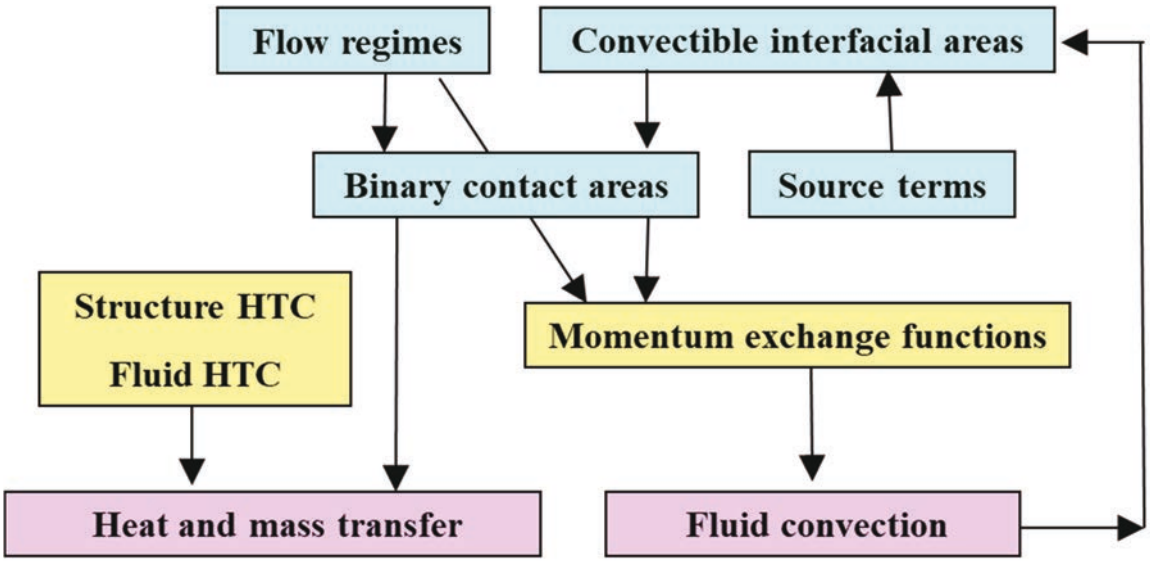

Fig. 1. Roles of the IFA model in SIMMER-III/SIMMER-IV.

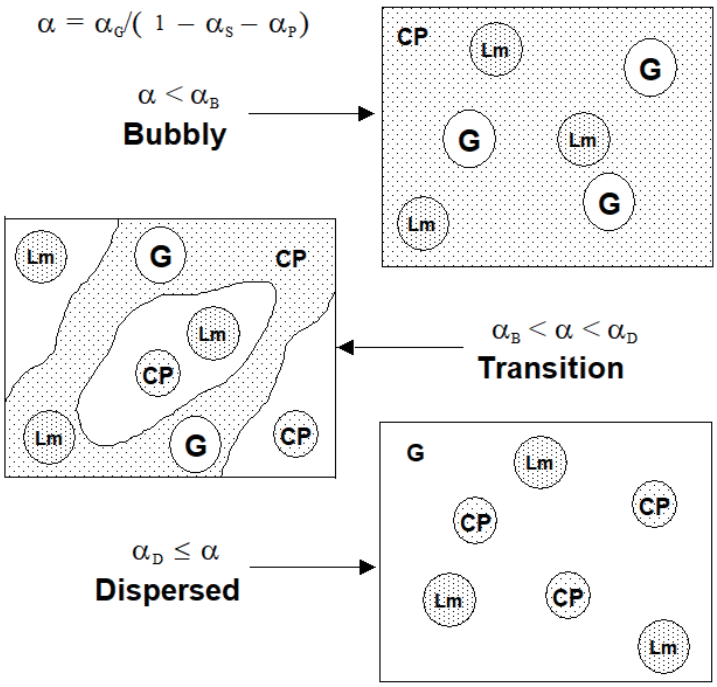

Fig. 2. Basic concept of multi-phase configuration in pool geometry.

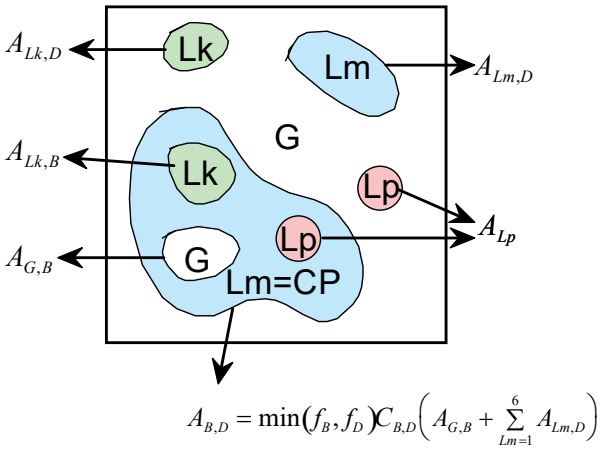

Fig. 3. Convectible interfacial areas modeled in SIMMER-III.

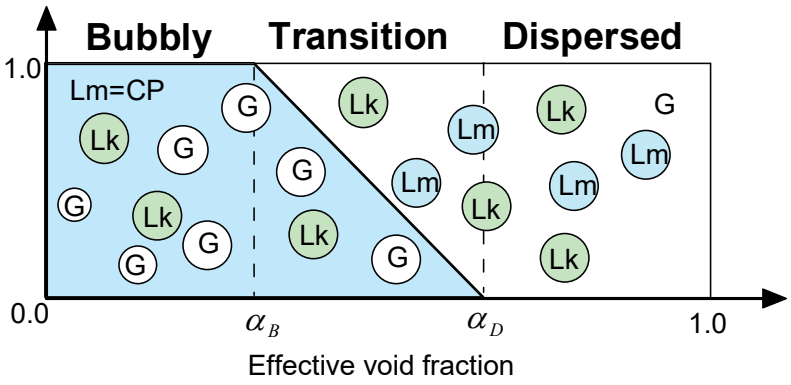

Fig. 4. Pool flow regime map represented in SIMMER-III.

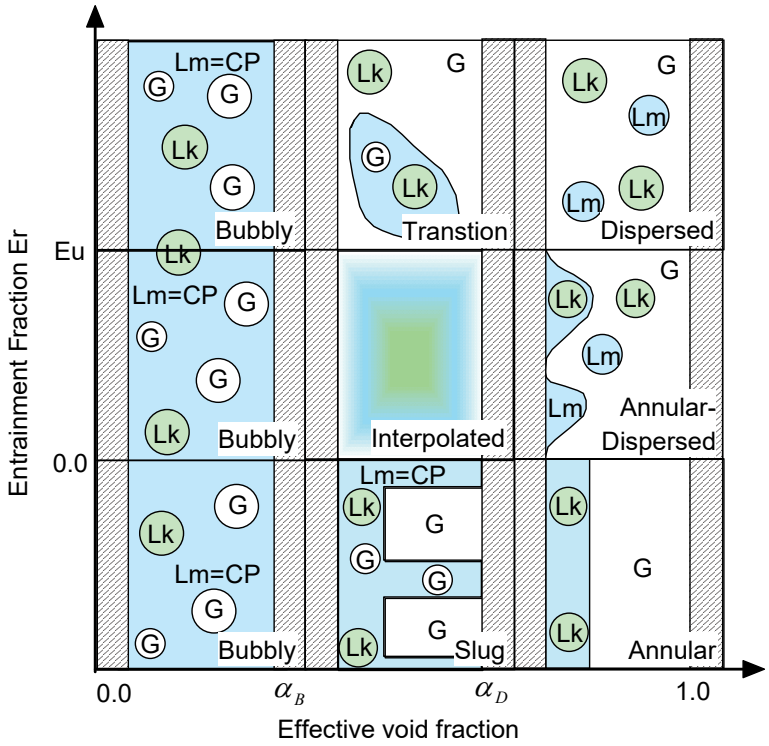

Fig. 5. Channel flow regime map in SIMMER-III.

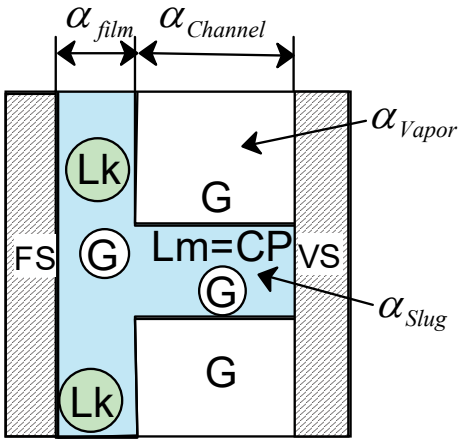

Fig. 6. Conceptual geometry of slug flow.

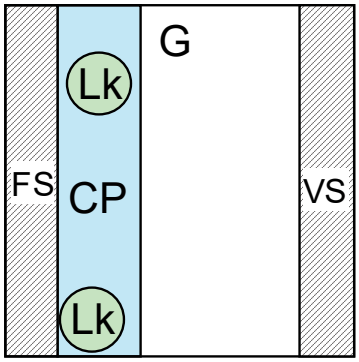

Fig. 7. Conceptual geometry of annular flow.

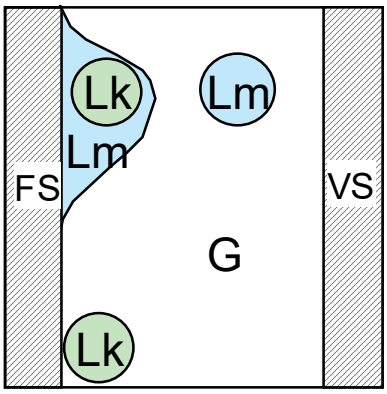

Fig. 8. Conceptual geometry of annular-dispersed flow.

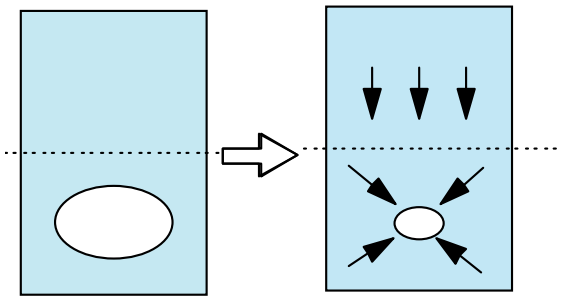

Fig. 9. Collapse of a bubble in a liquid pool.

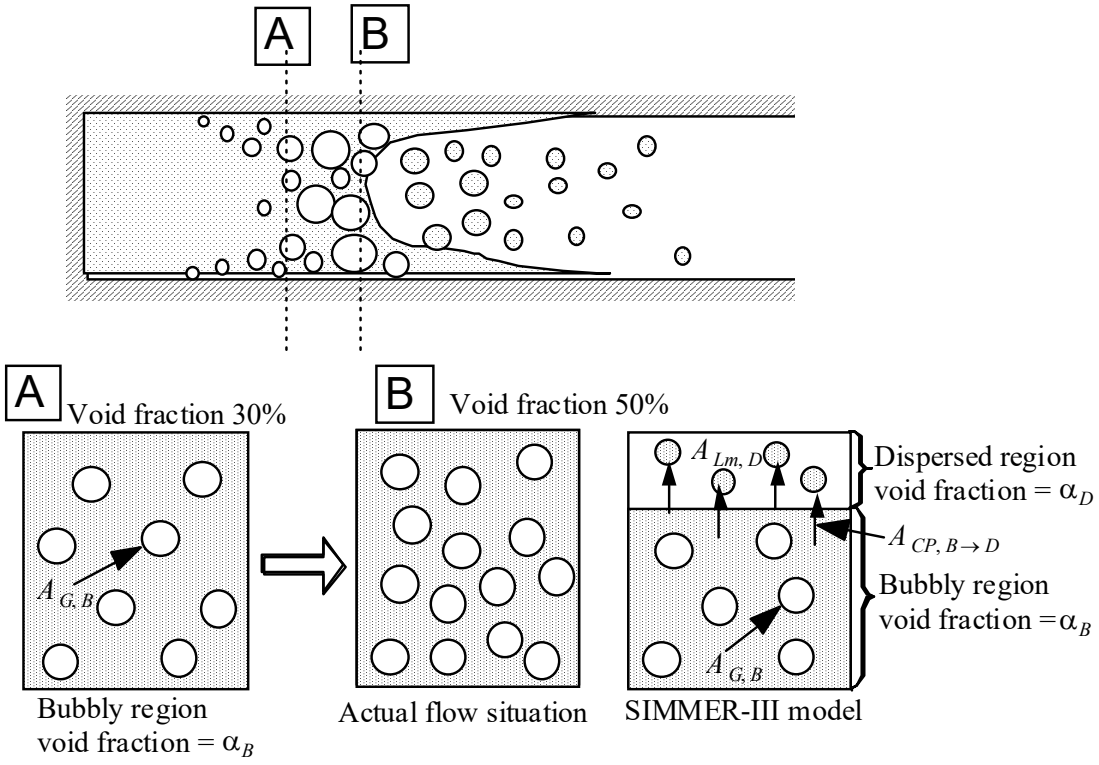

Fig. 10. Transient flow situation in the blowdown of high-pressure water to atmosphere (Edward's pipe experiment).

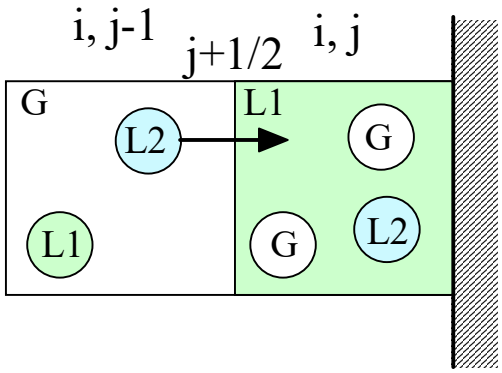

Fig. 11. Interfacial area convection between the cells with different topologies.

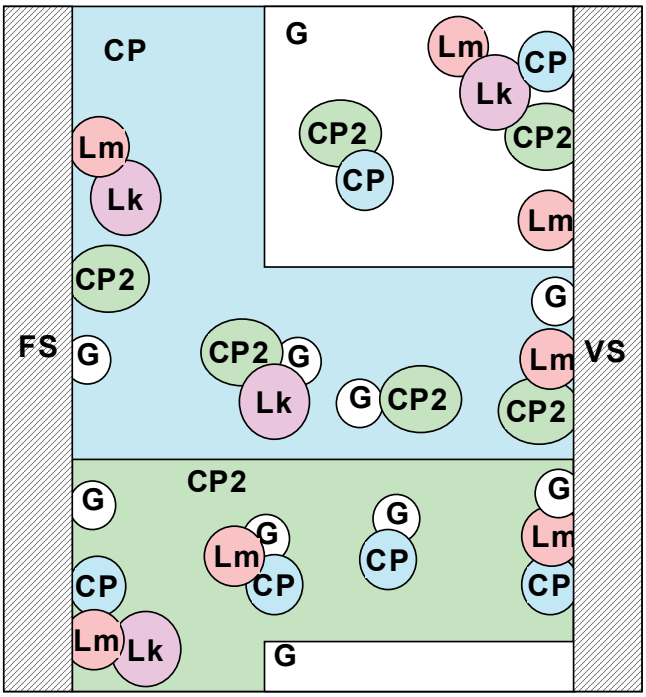

Fig. 12. Possible contact modes in SIMMER-III.

Appendix A: Division of Flow Area

To smoothen the flow regime transition, the physical quantities divided into the bubbly and dispersed regions must be appropriately averaged between the two. In the bubbly region, the liquid forms a continuous phase, whereas the vapor forms a continuous phase in the dispersed region. The volume fractions of these two regimes are determined from two requirements. First, the bubbly region has a local vapor volume fraction of α_B and the dispersed region α_D, where α_B and α_D are user-defined parameters. The effective vapor volume fraction is defined by

$$\alpha = \frac{\alpha_G}{1-\alpha_S-\alpha_P}. \tag{A-1}$$

Second, the real liquids and particles should be partitioned between the two regions with a same fraction.

The geometrical description of the division of flow area is shown in Fig. A-1. Two independent parameters are required to meet the two requirements described above. These are

f_B : the volume fraction of the bubbly region, and

X_B : the fraction of liquid components in the bubbly region.

The same fractions for the dispersed flow are obtained by subtracting these fractions from unity:

$f_D = 1 - f_B$: the volume fraction of the dispersed region, and

$X_D = 1 - X_B$: the fraction of liquid components in the dispersed region.

The requirements are described in the following equations:

$$f_B\alpha_F - X_B(\alpha_L+\alpha_P) = \alpha_B(f_B\alpha_F + X_B\alpha_P)\text{, and} \tag{A-2}$$

$$f_D\alpha_F - X_D(\alpha_L+\alpha_P) = \alpha_D(f_D\alpha_F + X_D\alpha_P), \tag{A-3}$$

where α_L is the total real liquid volume fraction,

α_P is the total particle volume fraction,

α_S is the structure volume fraction, and

$\alpha_F = (1-\alpha_S)$ is the volume fraction of the area that is available for flow.

By solving Eqs. (A-2) and (A-3), we obtain, after some algebraic manipulation,

$$f_B = \left\{1 + \frac{\alpha_P(\alpha^* - \alpha_B)}{\alpha_F(1-\alpha^*)}\right\}\frac{(\alpha_D - \alpha^*)}{(\alpha_D - \alpha_B)}, \tag{A-4}$$

$$f_D = \left\{1 + \frac{\alpha_P(\alpha_D - \alpha^*)}{\alpha_F(1-\alpha^*)}\right\}\frac{(\alpha^* - \alpha_B)}{(\alpha_D - \alpha_B)}, \tag{A-5}$$

$$X_B = \frac{(1-\alpha_B)(\alpha_D - \alpha^*)}{(\alpha_D - \alpha_B)(1-\alpha^*)}\text{, and} \tag{A-6}$$

$$X_D = \frac{(1-\alpha_D)(\alpha^* - \alpha_B)}{(\alpha_D - \alpha_B)(1-\alpha^*)}, \tag{A-7}$$

where $\alpha^* = \max[\alpha_B,\ \min(\alpha, \alpha_D)]$ is defined to make these equations applicable to the whole range of effective void fraction.

If solid particles are not present, Eqs. (A-4) and (A-5) reduce to simple linear fractions. The deviation from the simple linear fraction stems from the effective void fraction, which is defined as the vapor volume fraction to the total volume fraction of vapor and real liquids.

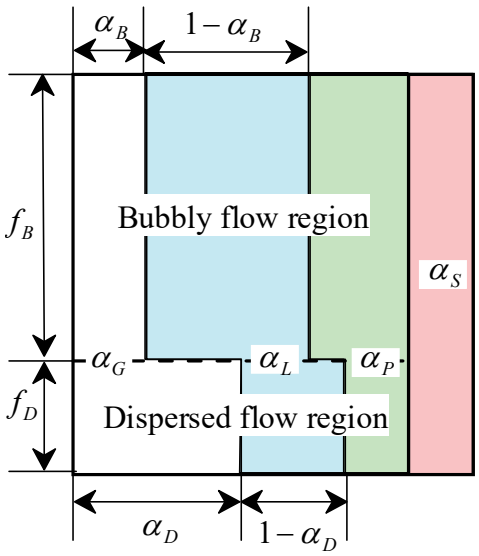

Fig. A-1. The schematic picture of the division of flow area in SIMMER-III.

Appendix B: Subdivision of Bubbly Flow Region

An abrupt change of IFAs may occur when a continuous phase changes to other components. To ensure the smooth transition of *CP* in this situation, a real liquid that has the second largest volume fraction and belongs to a velocity field different from *CP* is defined as the second continuous phase *CP*2. In order not to introduce excess complexity, the second continuous phase is calculated after all the convectible IFAs are updated and the bubbly flow region is subdivided into the *CP*-continuous region (subscripted *B*1) and the *CP*2-continuous region (subscripted by *B*2). The remaining real liquid is defined as the dispersed phase subscripted by *DP*. Figure B-1 shows the geometrical configuration of *CP*, *CP*2, and *DP*.

The definitions of the variables needed in this modeling are as follows.

$$\alpha_{CP2,eff} = \frac{\alpha_{CP2,B}}{\alpha_{CP,B} + \alpha_{CP2,B}}, \tag{B-1}$$

= Local effective volume fraction of component *CP*2,

$$\alpha^*_{CP2} = \max\left(\alpha_{B1},\ \min\left(\alpha_{CP2,eff}, \alpha_{B2}\right)\right), \tag{B-2}$$

= Local effective volume fraction of component *CP*2 with the limiting value,

$\alpha_{CP2,eff} \leq \alpha_{B1}$ describes the CP-continuous regime ,

$\alpha_{CP2,eff} \geq \alpha_{B2}$ describes the $CP2$-continuous regime , and

$\alpha_{B1} < \alpha_{CP2,eff} < \alpha_{B2}$ describes the transition regime .

The volume fractions to specify the boundaries, α_{B1} and α_{B2} , are input data. From the experimental data of water bubbling in mercury, the default value for α_{B1} is set to be 0.3, whereas 0.7 appears appropriate for α_{B2}.

The bubbly flow region is divided into two parts:

$$f_{B1} = \frac{\alpha_{B2} - \alpha^*_{CP2}}{\alpha_{B2} - \alpha_{B1}}, \tag{B-3}$$

= Fraction of *CP*-continuous (*B*1) region, and

$$f_{B2} = \frac{\alpha^*_{CP2} - \alpha_{B1}}{\alpha_{B2} - \alpha_{B1}}, \tag{B-4}$$

= Fraction of *CP*2-continuous (*B*2) region.

The *B*1 region has a local *CP*2 volume fraction of α_{B1} whereas the *B*2 region has a local *CP*2 volume fraction of α_{B2}. The dispersed liquid components (*m* = *DP*, 4, 5, 6, 7) and the vapor component are assumed to distribute uniformly in the bubbly region.

Some additional definitions can be made using these fractions as follows.

$$\alpha_{CP,B1} = \begin{cases} \alpha_{CP,B} & \text{for } \alpha_{CP2,eff} < \alpha_{B1} \\ f_{B1}(\alpha_{CP,B} + \alpha_{CP2,B})(1 - \alpha_{B1}) & \text{for } \alpha_{CP2,eff} \geq \alpha_{B1} \end{cases}, \quad \text{(B-5)}$$

= Volume fraction of *CP* in the *CP*-continuous region,

$$\alpha_{CP,B2} = \begin{cases} f_{B2}(\alpha_{CP,B} + \alpha_{CP2,B})(1 - \alpha_{B2}) & \text{for } \alpha_{CP2,eff} \leq \alpha_{B2} \\ \alpha_{CP,B} & \text{for } \alpha_{CP2,eff} > \alpha_{B2} \end{cases}, \quad \text{(B-6)}$$

= Volume fraction of *CP* in the *CP*2-continuous region,

$$\alpha_{CP2,B1} = \begin{cases} \alpha_{CP2,B} & \text{for } \alpha_{CP2,eff} \leq \alpha_{B1} \\ f_{B1}(\alpha_{CP,B} + \alpha_{CP2,B})\alpha_{B1} & \text{for } \alpha_{CP2,eff} > \alpha_{B1} \end{cases}, \quad \text{(B-7)}$$

= Volume fraction of *CP*2 in the *CP*-continuous region,

$$\alpha_{CP2,B2} = \begin{cases} f_{B2}(\alpha_{CP,B} + \alpha_{CP2,B})\alpha_{B2} & \text{for } \alpha_{CP2,eff} \leq \alpha_{B2} \\ \alpha_{CP2,B} & \text{for } \alpha_{CP2,eff} > \alpha_{B2} \end{cases}, \quad \text{(B-8)}$$

= Volume fraction of *CP*2 in the *CP*2-continuous region,

$$\alpha_{Lm,B1} = f_{B1}\alpha_{Lm,B} \quad \text{for } m=DP, 4, 5, 6, 7\,, \quad \text{(B-9)}$$

= Volume fraction of dispersed liquid components in the *CP*-continuous region, and

$$\alpha_{Lm,B2} = f_{B2}\alpha_{Lm,B} \quad \text{for } m=DP, 4, 5, 6\,, \quad \text{(B-10)}$$

= Volume fraction of dispersed liquid components in the CP2-continuous region.

The convectible IFA of component *CP*2 in the *CP*-continuous region is assumed to be proportional to the volume fraction as follows

$$A_{CP2,B1} = \frac{\alpha_{CP,B1}}{\alpha_{CP2,B}} A_{CP2,B}\,. \quad \text{(B-11)}$$

The IFA between component *CP* and *CP*2 must be conserved. Hence the reasonable definition for the IFA of component *CP* in *CP*2-continuous region is

$$A_{CP2,B2} = A_{CP2,B} - A_{CP2,B1}\,. \quad \text{(B-12)}$$

The IFA between *CP*-continuous and *CP*2-continuous regions is assumed to be zero. The same procedure as used in defining $A_{B,D}$ is possible, but it is not applied to this case because the present formulation is only a mathematical interpolation between the flow regimes with different continuous phases. The remaining IFAs of *CP* and *CP*2 are set to zero similar to $A_{CP,B}$. These are

$$A_{CP,B1} = 0\,, \text{and} \quad \text{(B-13)}$$

$$A_{CP2,B2} = 0\,. \quad \text{(B-14)}$$

The convectible areas of dispersed liquid components and the surface areas of structures in the bubbly flow region are divided into the *CP*-continuous and *CP*2-continuous regions using the fractions f_{B1} and f_{B2}:

$$A_{FS,B1} = f_{B1} A_{FS,B} \,, \tag{B-15}$$

$$A_{FS,B2} = f_{B2} A_{FS,B} \,, \tag{B-16}$$

$$A_{VS,B1} = f_{B1} A_{VS,B} \,, \tag{B-17}$$

$$A_{VS,B2} = f_{B2} A_{VS,B} \,, \tag{B-18}$$

$$A_{Lm,B1} = f_{B1} A_{Lm,B} \quad \text{for } m=DP, 4, 5, 6, 7 \,, \text{and} \tag{B-19}$$

$$A_{Lm,B2} = f_{B2} A_{Lm,B} \quad \text{for } m=DP, 4, 5, 6, 7 \,. \tag{B-20}$$

This second continuous phase modeling, with appropriate averaging procedure of momentum exchange functions, can eliminate an abrupt change of flow properties at the continuous phase transition.

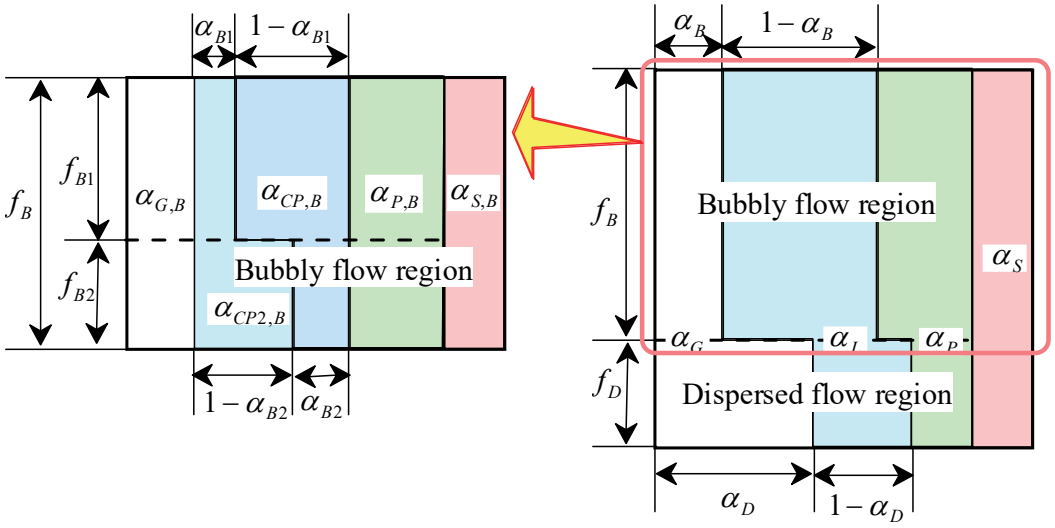

Fig. B-1. Subdivision of the bubbly flow area into CP-continuous and CP2-continuous regions.

Appendix C: Entrainment Fraction

An approach, which formulates the flow regime transition based on a time-dependent entrainment fraction E_r is proposed.[15), 16)] The stability upon the flow regime transition is significantly improved by calculating the evolution of E_r expressed by a differential equation. An equation is proposed to have an equilibrium value and a time constant,

$$\frac{\partial E_r}{\partial t} = \frac{1}{\tau_{en}}(E_e - E_r)\,, \tag{3-44}$$

where E_e is the equilibrium entrainment fraction for given flow conditions, and
τ_{en} is the entrainment time constant.

Three regions are proposed to exist. The $E_r = 0$ region corresponds to the bubbly, slug and annular flow. The $0 < E_r < E_u$ region corresponds to the bubbly, interpolated and annular-dispersed flow. The $E_r = E_u$ region corresponds to the bubbly, pool transition and dispersed flow.

The upper limit of the entrainment fraction E_u is defined as the fraction of the vapor-"film" structure contact area to the total "film" structure IFA as

$$E_u = \frac{a_{G,FS}}{A_{FS}}, \tag{C-1}$$

where

$$a_{G,FS} = C_{G,S}\frac{\alpha_{G,B}}{\alpha_{F,B}}\min\left(A_{G,B}, A_{FS}\right) + \max\left[C_{G,S}\frac{\alpha_{G,D}}{\alpha_{F,D}}A_{FS,D}, A_{FS,D} - \sum_{Lm=1}^{6} C_{Lm,S}\frac{\alpha_{Lm,D}}{\alpha_{F,D}}\min\left(A_{Lm,D}, A_{FS,D}\right)\right]. \tag{C-2}$$

A simple flooding criterion is used, above which the entrainment is assumed to occur and Eq. (3-44) is used to calculate E_r. The criterion is expressed in terms of a dimensionless number:[9)]

$$j_G^* = \frac{\alpha_G}{1-\alpha_S}|\vec{v}_G|\sqrt{\frac{\rho_G}{gD_h(\rho_L - \rho_G)}}, \tag{C-3}$$

where g is the invariant gravitational acceleration,
D_h is the hydraulic diameter,
ρ_G is the microscopic density of vapor,
ρ_L is the average microscopic density of liquid, defined as

$\rho_L = \sum_m \bar{\rho}_{Lm}/(\alpha_L + \alpha_P)$, and

$\vec{v}_G$ is the vapor velocity.

It is proposed to formulate a hysteresis effect for stability, because the liquid-vapor coupling changes more than an order of magnitude upon the flooding initiation. The proposed formulation is as follows,

$$\begin{cases} E_r = 0 \rightarrow E_r > 0 & \text{if } j_G^* > j_{Begin}^* = 1.2 \text{ (default)} \\ E_r = 0 \leftarrow E_r > 0 & \text{if } j_G^* < j_{Stop}^* = 0.4 \text{ (default)} \end{cases} . \tag{C-4}$$

Ishii and Mishima[15] proposed the equilibrium entrainment fraction E_e to be given by

$$E_e = \tanh\left(7.25 \times 10^{-7} \mathrm{We}^{1.25} {\mathrm{Re}_f}^{0.25}\right), \tag{C-5}$$

where We is Weber number for entrainment and Re_f is the total liquid Reynolds number. These are defined by

$$\mathrm{We} = \rho_G \left(\frac{\alpha_G}{1-\alpha_S}|\vec{v}_G|\right)^2 D_h \frac{1}{\sigma_{CP}} \left(\frac{\rho_L - \rho_G}{\rho_L}\right)^{\frac{1}{3}}, \text{and} \tag{C-6}$$

$$\mathrm{Re}_f = \sum_{Lm=1}^{3} \frac{\bar{\rho}_{Lm}|\vec{v}_{Lm}|D_h}{\mu_{Lm}(1-\alpha_S)}, \tag{C-7}$$

where σ_{CP} is the surface tension of the continuous liquid phase,
$\vec{v}_{Lm}$ is the velocity of liquid-component m, and
μ_{Lm} is the viscosity of liquid-component *m* (the particles are assumed to have an infinite viscosity and excluded from the summation).

The hyperbolic tangent in Eq. (C-5) can be omitted because large vapor velocity is required to obtain the upper limit of Eq. (C-2). In addition, E_e should be multiplied by an additional factor to reach the correct limit of the dispersed flow when only the particles exist. The proposed formula is

$$E_e = C_{E1} \mathrm{We}^{C_{E2}} {\mathrm{Re}_f}^{0.25} \Big/ \left(\frac{\alpha_L}{\alpha_L + \alpha_P}\right)^{C_{E3}} . \tag{C-8}$$

The time constant is adopted from Kataoka et al.[16] as

$$\tau_{en} = C_{E4} \frac{\sum_{Lm=1}^{3} \bar{\rho}_{Lm}}{\phi_f (\alpha_L + \alpha_P) \alpha_{S,PIN}} \left(\frac{\phi_f D_h}{\mu_G}\right)^{0.26}, \tag{C-9}$$

where μ_G is the vapor viscosity, and

$$\phi_f = \sum_{Lm=1}^{6} \bar{\rho}_{Lm} |\vec{v}_{Lm}| \frac{1}{1-\alpha_S}. \tag{C-10}$$

The coefficients C_{E1}, C_{E2}, C_{E3} and C_{E4} are user-defined parameters and their default values are $C_{E1} = 7 \times 10^{-7}$, $C_{E2} = 1.25$, $C_{E3} = 1.0$, and $C_{E4} = 45$.

Appendix D: Test Calculations of the Compression Term

As discussed in Section 4.2, IFAs may change with fluid compression. Equation (4-23) is implemented to model the compression term in SIMMER-III. In this appendix, two sample problems are described to confirm its validity and effect. The first problem is the collapse of a bubble due to the motion of a liquid slug. A fuel vapor bubble in the liquid fuel pool was modeled as 1-D geometry with 2 axial mesh cells as shown in Fig. D-1.

The lower cell contains a fuel vapor bubble with the volume fraction of 20%, the radius of 0.02 m, and the IFA per unit volume of 30.0 m^{-1}. The upper cell is filled with single-phase liquid fuel. The initial temperature of the liquid fuel and vapor is 3200 K. A constant pressure of 1.0 MPa is applied to the top boundary and then the bubble collapses within 35 ms by the downward fluid motion driven by the pressure gradient as shown in Fig. D-2. Two parametric cases were run for this test case: the case with the proposed IFA convection equation and the case with the original equation. The change of bubble radius and IFA were plotted in Figs. D-3 and D-4, respectively, with the theoretical value which are deduced from the change of volume fraction of the bubble. The bubble radius should be proportional to the 1/3-rd power of the volume and the IFA to the 2/3-rd power. The results of the proposed equation show good agreement with the theoretical values whereas the results of original convection equation give constant IFA and very small bubble radius.

The second sample problem is the rise of a bubble by buoyancy. A bubble is placed at the bottom of a single-phase pool and rises by buoyant force. This situation was modeled as 1-D geometry with 20 axial mesh cells as shown in Fig. D-5. The bottom mesh cell contains a fuel vapor bubble with the volume fraction of 20%, the radius of 0.02 m, and the IFA per unit volume of 30.0 m^{-1}. The remaining mesh cells are filled with single-phase liquid fuel. The initial temperature of the liquid fuel and vapor is 3200 K. The bubble rises by buoyant force as shown in Fig. D-6.

Two cases, with the proposed convection equation and with the original equation, were run. The calculated void fraction and the radius of the bubbles are averaged over the system and plotted in Figs. D-7 and D-8, respectively. The theoretical radius and IFA deduced from the change of bubble volume are also plotted in these figures. The agreement between the theoretical value and the result of the original equation is poor. The case with the proposed equation better follows the theoretical prediction of the increase of IFA due to bubble expansion qualitatively. However, the case is not yet satisfactory, because the effect of numerical diffusion cannot be eliminated even with the higher-order differencing scheme.

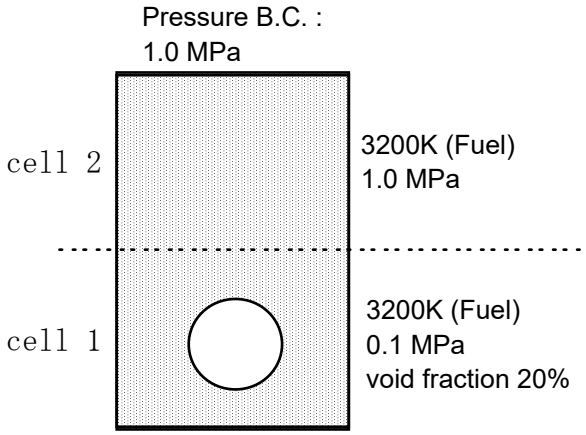

Fig. D-1. Sample problem No.1: bubble collapse by liquid slug.

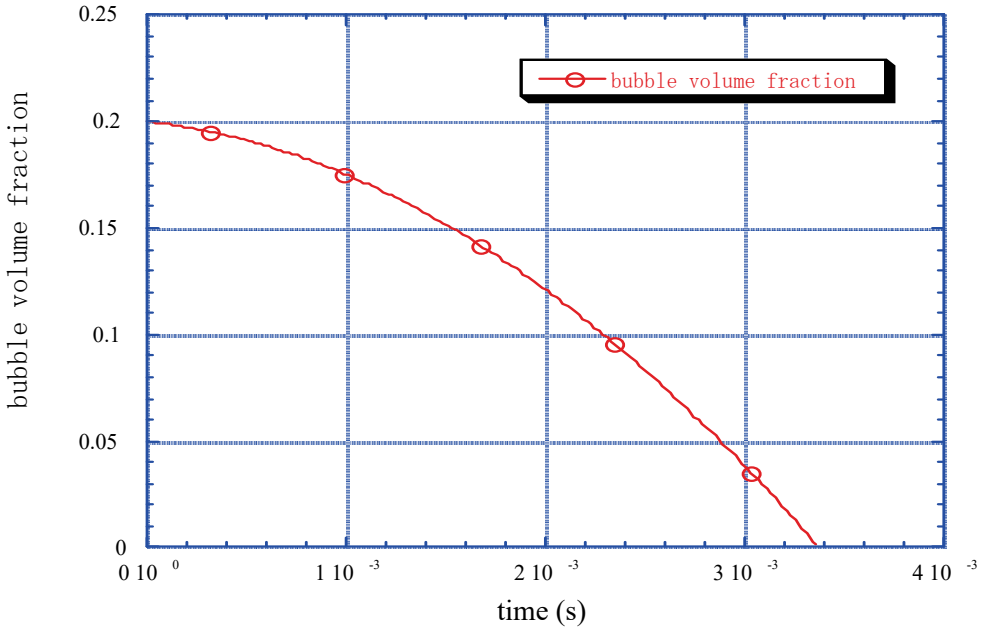

Fig. D-2. Bubble collapse by liquid slug.

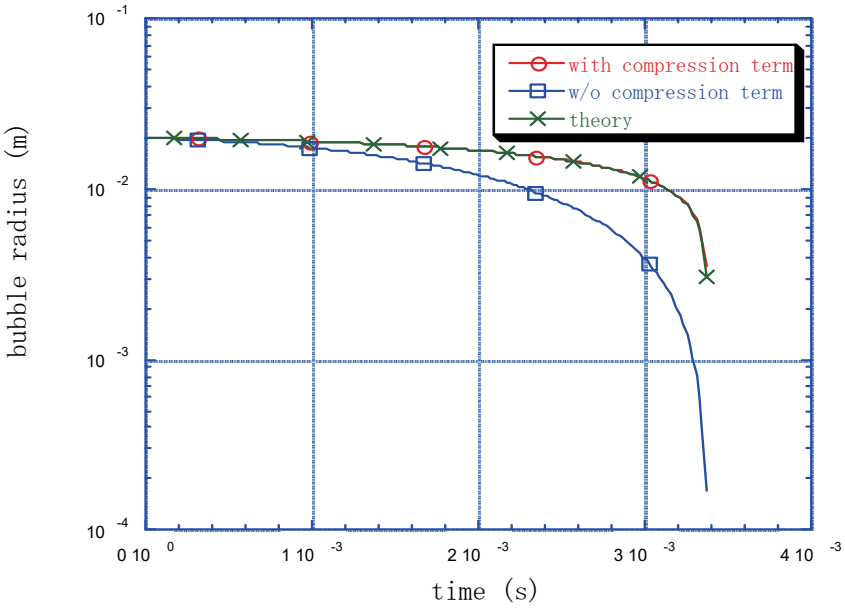

Fig. D-3. Transient of bubble radius.

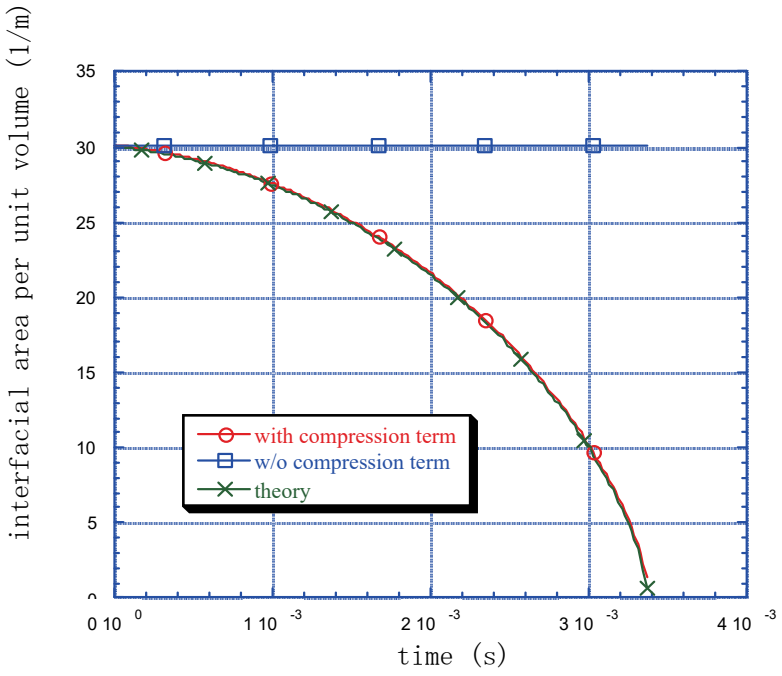

Fig. D-4. Transient of bubble interfacial area per unit volume.

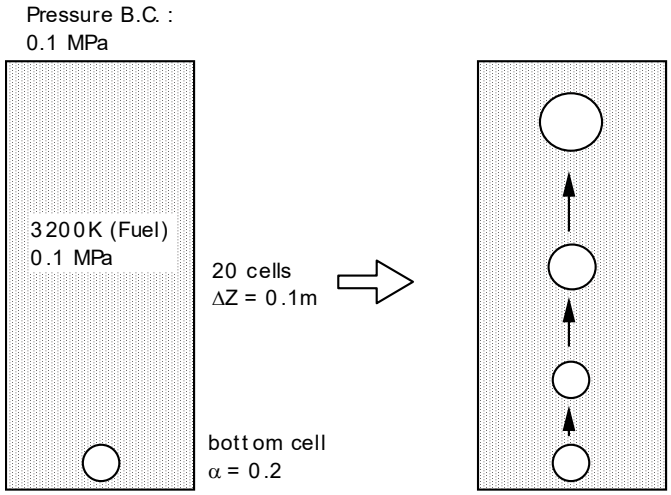

Fig. D-5. Sample problem No.2: buoyant rise of a bubble in fuel pool.

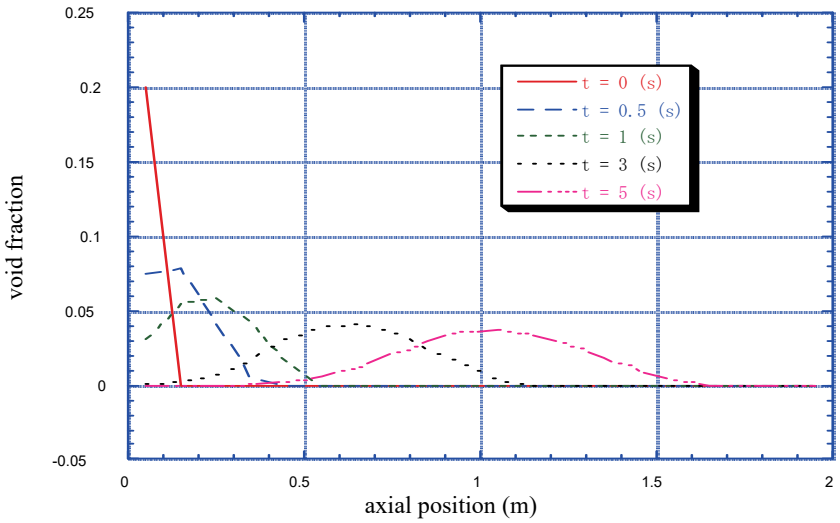

Fig. D-6. Transient change of the void fraction distribution.

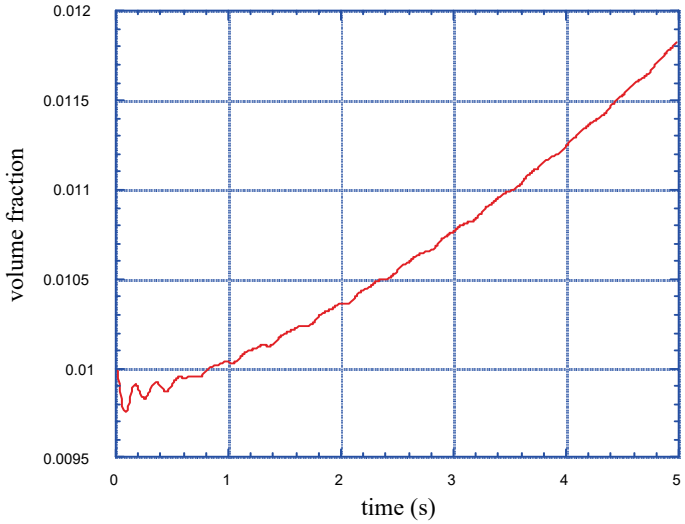

Fig. D-7. Transient change of the bubble volume.

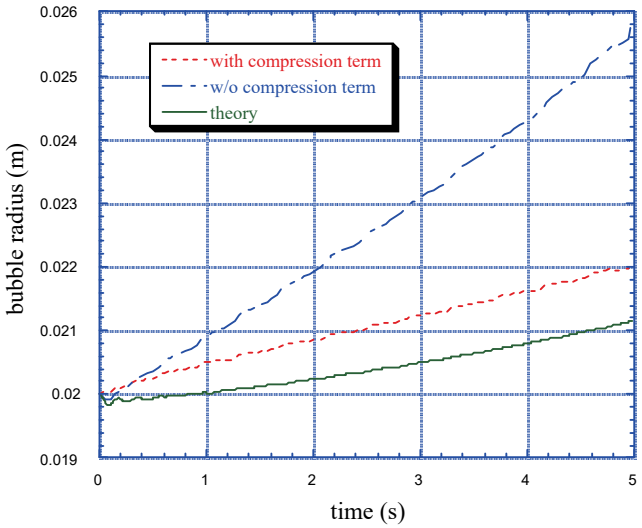

Fig. D-8. Transient change of bubble radius.

This is a blank page.